

This manuscript is a preprint and will be submitted to the Journal of Sedimentary Research (JSR). This manuscript has not undergone peer review. Subsequent versions of this manuscript may have different content. If accepted, the final peer-reviewed version of this manuscript will be available via the 'Peer-reviewed Publication' DOI link on the right-hand side of this webpage. Please feel free to contact any of the authors directly to comment on the manuscript.

Lateral variability of shelf-edge, slope and basin-floor deposits, Santos Basin, offshore Brazil

Michael J. Steventon^{1*}, Christopher A-L. Jackson¹, David M. Hodgson² & Howard D. Johnson¹

¹Basins Research Group (BRG), Department of Earth Science & Engineering, Imperial College, Prince Consort Road, London, SW7 2BP, UK

²School of Earth and Environment, University of Leeds, Leeds, LS2 9JT, UK

Contact: michael.steventon13@imperial.ac.uk

WORD COUNT: 9247 (main body), 1056 (figure captions), 2708 (references)

ABSTRACT

Construction of continental margins is driven by sediment transported across the shelf to the shelf-edge, where it is reworked by wave-, tide- and river-influenced processes within deltas and flanking clastic shorelines. Stalling of continental margin progradation often results in degradation of the outer shelf to upper slope, with re-sedimentation to the lower slope and basin-floor via a range of sediment gravity-flows and mass-movement processes. Our understanding of how these processes contribute to the long-term development of continental margins has typically been limited to observations from broadly two-dimensional, subsurface and outcrop datasets. Consequently, the three-dimensional, particularly along-strike variability in process regime and margin evolution is poorly constrained and often underappreciated. We use a large (90 km by 30 km, parallel to depositional strike and dip, respectively) post-stack time-migrated 3D seismic-reflection dataset to investigate along-strike variations in shelf margin progradation and outer-shelf to upper-slope collapse in the Santos Basin, offshore SE Brazil. Early Palaeogene to Eocene progradation of the shelf margin is recorded by spectacularly imaged, SE-dipping clinoforms. Periodic failure of the outer-shelf and upper slope formed *c.* 30 km-wide (parallel to shelf margin strike) slump scars, which resulted in a strongly scalloped upper slope. Margin collapse caused (1) the emplacement of slope-attached mass-transport complexes (MTCs) (up to *ca.* 375 m thick, 12+ km long, 20 km wide) on the proximal basin-floor, and (2) accommodation creation on the outer shelf to upper slope. This newly formed accommodation was infilled by shelf-edge-delta clinoforms (up to 685 m thick), that nucleated and

prograded basinward from the margin-collapse headwall scarp, downlapping onto the underlying slump scar and/or MTCs. Trajectory analysis of the shelf-edge deltas suggests that slope degradation-created accommodation was generated mainly during times of base-level rise rather than, as would be predicted by most sequence-stratigraphic models, during base-level fall. Our results highlight the significant along-strike variability in depositional style, geometry and evolution of that can occur on this and other continental margins. Coeval strata, separated by only a few kilometres, display strikingly different stratigraphic architectures; this variability could be missed in 2D datasets and is not currently captured in conventional 2D sequence stratigraphic models.

Keywords: shelf-edge deltas, mass-transport complexes/deposits (MTC/MTD), toe-of-slope fans, continental margins, sequence stratigraphy, clinof orm, clinothem, trajectory analysis

INTRODUCTION

Shelf-edges are dynamic areas of erosion, deposition, degradation, and sediment bypass, forming the staging area for deep-water deposits. The principal accretionary unit of basin margins, the clinothem (bounded by clinoforms), records the interplay between shallow-marine and slope-related/gravitational processes, and fluctuations in sediment supply, relative sea-level, and accommodation. Since there are no accessible modern analogues, due to the Holocene transgression, our understanding of shelf-edge/basin margin settings relies heavily on subsurface data, augmented by the development of sequence stratigraphic concepts (Mitchum et al. 1977; Vail et al. 1977; Weimer 1989; Van Wagoner et al. 1990; Hunt & Tucker 1992; Posamentier et al. 1992; Catuneanu 2006; Neal et al. 2016). These concepts have been extended further through shelf-edge (shoreline) trajectory analysis, which considers the influence of sediment supply and relative sea-level changes on the stratigraphic architecture and facies distributions along shelf-edges (Helland-Hansen & Gjelberg 1994; Helland-Hansen & Martinsen 1996; Steel & Olsen 2002; Carvajal et al. 2009; Helland-Hansen & Hampson 2009). However, the role of outer-shelf to upper-slope degradation and along-strike depositional variability on shelf-edge development, and their coupled impact on sequence-stratigraphic models, has received less attention (e.g. Neal & Abreu 2009). This partly reflects the fact that deposits and shelf-edge trajectories associated with degradational phases are poorly preserved and because most studies are largely two-dimensional (2-D). There have been recent re-assessments of concepts such as along-strike variability (Madof et al. 2016) and three-dimensionality (Burgess 2016) in shelf-edge process and product (Deibert et al. 2003; Dixon et al. 2012; Cosgrove et al. 2018), and the general non-uniqueness of stratigraphic patterns when trying to determine autocyclic versus allogenic controls (Muto et al. 2007; Burgess & Prince 2015; Hampson 2016). In this light, there is also a case for reevaluating margins characterised by significant degradational phases, and along-strike variability in depositional system type and stratigraphic architecture (Fig.1).

Shelf-edges with degradational phases form through a combination of pre-conditioning factors (e.g. slope over-steepening, relative sea-level change, mobile substrates, etc.), which cause the upper slope gradient to exceed a stable equilibrium (e.g. Ross et al. 1994; Adams & Schlager 2000; Locat & Lee 2002; Sultan et al. 2004; Prather et al. 2017). These out-of-grade systems can achieve grade by the outer-shelf to upper-slope failing, resulting in the downdip deposition mass-transport complexes/deposits (MTCs) and the formation of canyon- or channel-like sediment conduits (Galloway 1998). Degradational-influenced sequences are generally characterised by a repetitive cycles of (i) shelf-edge to upper-slope failure and the formation of erosive scarps (60 km in width, up to 825 m in height), (ii) deposition of base-of-slope MTCs that may onlap landward against previously deposited slope deposits, (iii) further mass-wasting and

sediment bypass, and (iv) infilling or “healing” of the evacuated area by shelf-edge (e.g. Gomis-Cartesio et al. 2018; Proust et al. 2018). Although there are exceptions (e.g. McMurray & Gawthorpe 2000; Jones et al. 2015), most stratigraphic models that document some form of shelf-edge failure are based on predominantly 2-D datasets, most typically from outcrop (e.g. Dixon et al. 2013; Peng et al. 2017; Gomis-Cartesio et al. 2018) and therefore are only capturing a snapshot of the system architecture, and not the full along-strike variability.

The principle aim of this study is to (i) characterise a shelf-edge during multiple periods of progradation and degradation, and (ii) determine the geological controls on the lateral variability of the Paleocene-Eocene outer shelf to slope depositional system in the Santos Basin, offshore Brazil (Fig. 2). This is achieved through a detailed seismic facies analysis of a 3D seismic-reflection dataset, which provides continuous high-quality imaging of an area extending for *ca.* 90 km along depositional strike and *ca.* 30 km along depositional dip. The main objectives are to: (i) describe the distribution of depositional elements along the full along-strike length of the margin during multiple phases of construction and degradation, (ii) use clinof orm trajectory analysis to characterise sediment partitioning relationships between the shelf-edge and basin-floor, (iii) evaluate the potential driving mechanisms for periodic shelf-edge collapse, and (iv) develop a predictive, three-dimensional stratigraphic model for margins with constructional and degradational phases.

BASIN SETTING

The Santos Basin is located within the Central Segment of the South Atlantic (Fig. 2), bound to the north by the Cabo Frio High and to the south by the Florianópolis Fracture Zone (Meisling et al. 2001; Torsvik et al. 2009). The basin formed in response to the Gondwanan break-up cycle, which propagated from the south, reaching the Florianópolis Fracture Zone during the Early Cretaceous (e.g. Clemson et al. 1997; Meisling et al. 2001; Karner & Gambôa 2007; Mohriak et al. 2008). The tectono-stratigraphic evolution of the basin is defined by four megasequences (Fig. 3): (i) a syn-rift phase (Hauterivian-Aptian), (ii) a transitional “sag” phase (Aptian) (i.e. earliest post-rift), during which time a thick (up to 2.5 km; Davison et al., 2012) evaporite-dominated sequence was deposited, (iii) a restricted marine phase (Albian) (i.e. early post-rift), and (iv) a fully marine, passive margin phase (Cenomanian-present) (i.e. main post-rift phase) (Chang et al. 1992; Meisling et al. 2001; Guerra & Underhill 2012). This study focuses on the Paleogene period of the passive margin phase (Fig. 3).

From the Late Cretaceous to Early Paleogene, a thick clastic wedge prograded south-eastwards into the Santos Basin (Figs. 3 & 4) (Macedo 1989; Guerra & Underhill 2012). This sediment flux was driven by periodic regional uplift of the onshore Serra do Mar and Serra da Mantiqueira coastal ranges (Cobbold et al. 2001; Saenz et al. 2003), which exceeded a global eustatic sea-level high, allowing sand-rich systems to prograde beyond the previous drowned Albian carbonate shelf (Modica & Brush 2004). Onshore tectonic readjustment in the latest Cretaceous to Early Paleocene, reorganised the drainage networks to have a NE trend (ancestral Paraíba do Sul river system), shifting the loci of sedimentation northwards towards the central and northern Santos Basins (Cobbold et al. 2001; Modica & Brush 2004; Duarte & Viana 2007). Shelf-edge deltas developed during the Paleocene in the central and northern Santos Basin (Fig. 2), while areas to the south were sediment starved (Modica & Brush 2004). The Eocene records continued progradation of shelf-edge deltas and forms the focus of this study. The succession is dissected by a middle-Eocene (40-43 Ma) erosion surface that formed due to large-scale collapse of the margin. This event remobilised material on the delta topsets and foresets, resulting in the deposition of MTCs and turbidites that form hydrocarbon-bearing reservoirs in the north of the basin (Fig. 2; Atlanta and Oliva fields) (Ebiwonjumi & Schwartz 2003). The Eocene shelf-edge deltas are capped by a regionally extensive Early Oligocene flooding surface (Fig. 3). This regionally mappable surface (see below) records a global marine highstand, which drove landward-directed back-stepping of the shelf-slope break by >35 km (Fig. 3).

From the late Paleogene to present-day, deposition in the central Santos Basin has been dominated by a contourite drift system (Duarte & Viana 2007). During this time, tectonic reorganisation of the onshore terranes resulted in diversion of the ancestral Paraíba do Sul river into the Campos Basin (Karner & Driscoll 1999). This is manifested in synchronous retrogradation and progradation of shorelines in the northern Santos (which was sediment starved) and Campos Basin (which was sediment nourished, being now fed by the Paraíba do Sul river), respectively. In the southern and central Santos Basin a new sediment source initiated during the Neogene, recorded by thick sediment packages (e.g. Williams & Hubbard 1984), renewed progradation, and widespread mass-wasting (Figs. 3 & 4).

DATASET & METHODS

Dataset

This study utilises a c. 3600 km², post-stack time migrated (PSTM) 3D seismic-reflection survey located within the Southern Embayment of the Santos Basin, offshore Brazil. The data straddle the modern day shelf-edge break between the Sao Paulo and Merluza transfer zones (SPTZ & MTZ) (Modica & Brush 2004) (Fig. 2). The data are SEG normal polarity (American polarity, i.e. an increase in acoustic impedance = peak), zero-phased, and have a processing bin spacing of 25×12.5 m. Vertical resolution (VR) within the Paleocene-Eocene interval of interest is c. 28 m, assuming a velocity of 2750 ms⁻¹ estimated from Berton & Vesely (2016) and dominant frequency of 24 Hz (extracted directly from the seismic data).

Seismic interpretation

The survey images the first four seconds two-way time (TWT) of post-salt succession (c. 5.5 km thick), including the main Paleocene-Eocene progradational phase. No wells were available, with ages and velocities estimated through calibration with regional studies (Modica & Brush 2004; Davison 2007; Berton & Vesely 2016). We map two basinwide flooding surfaces in this succession; approximately Maastrichtian-Paleocene (ca. 55-59 Ma) and Early Oligocene (ca. 30-35 Ma) in age. We also locally map an Eocene (ca. 40-43 Ma) erosional surface that is restricted to the outer shelf to upper slope of one of the clinothems developed within the Paleocene-Eocene progradational succession. We mapped top Aptian salt to determine potential structural (and related subsidence) controls on the style of margin progradation (see supplementary material). We used the following geometric-, amplitude- and frequency-based attributes to image the various depositional systems of interest: (i) variance (coherency) (see Van Bemmelen & Pepper 2000), (ii) root-mean squared (RMS) amplitude, and (iii) spectral decomposition (see Partyka et al. 1999) (frequency spectra can be found in the supplementary material).

Shelf-edge trajectory analysis

Shelf-edge trajectories define the spatial and temporal migration of clinoform rollover points during aggradation, progradation and retrogradation, and can be used to divide sedimentary units into discrete genetic packages (see Helland-Hansen & Martinsen 1996). Shelf-edge trajectories reflect the interplay between sediment supply and accommodation (see Helland-Hansen & Hampson 2009). They can aid prediction of sand supply to basin margins and reservoir presence in deep-water settings (e.g. Steel & Olsen 2002). The basin margin setting in our study area is characterised by the large clinoforms (ca. 275-685 m thick) that are composed of well-defined topsets (shelf), foresets (slope), and bottomsets (basin-floor). Clinoform rollover points separate low-angle (<1°) topsets from high-angle (up to 6°) foresets.

Shelf-edge trajectories are often grouped into three main categories: (i) rising-/ascending-seaward trajectories, reflecting highstand and/or normal regression, (ii) rising-/ascending-landward trajectories, reflecting coastal retrogradation (transgression), and (iii) falling-/flat trajectories, reflecting lowstand and/or forced regressive conditions (Posamentier et al. 1992; Helland-Hansen & Martinsen 1996; Helland-Hansen & Hampson 2009). Rising trajectories of both regressive and transgressive types can promote sediment storage on the shelf, whereas falling trajectories may (but need not always; e.g. Burgess & Hovius 1998; Carvajal & Steel 2006; Cosgrove et al. 2018) be related to shelf-incision, river mouth bypassing and delivery of sand-grade material to deep-water settings (e.g. Johannessen & Steel 2005).

In this study, the trajectory of the Paleogene-Eocene shelf-edge is obtained by plotting clinoform rollover points from six dip-oriented sections that are datumed on the Early Oligocene flooding surface (green-horizon), where it is located in a topset position. This surface was chosen as the datum because it is laterally extensive across the Eocene and Paleocene deltas and has only a minor basinward dip ($<1^\circ$ on the shelf directly above the clinoform rollover points) (Fig. 4). The clinoform rollover points (shelf-edge) are defined by geometrically linking two tangent lines from the topsets and foresets, finding the intersection, and then tracing orthogonally from these points.

Volumetric based sediment flux (Q)

Time-structure maps (Maastrichtian-Paleocene and Early Oligocene) were depth converted using estimated sediment velocities (*c.* 2750 ms^{-1}) (Berton & Vesely 2016). The resulting depth-structure maps were then decompacted to remove the effects of burial-related porosity reduction and hence provide an estimate of the pre-compaction thickness of the Maastrichtian-Paleocene to Early Oligocene time-interval (T_a). The time-interval represented by these units is based on estimates of the ages of the bounding surfaces, which are themselves estimated from data presented by Modica & Brush (2004). The decompacted volume was used to estimate the gross sediment flux (Q) for the study area, along with the change along strike of the shelf-edge from north to south. The resulting values of sediment flux are minimum estimates, given the incomplete imaging of the complete depositional system (i.e. distal basin-floor and uppermost coastal plain). Specifics of the calculations are detailed in the supplementary material, with the first-order sediment flux estimated by:

$$Q = \frac{V_c \times D}{T_a} \quad (1)$$

D = compaction correction (see Supplementary material).

SEISMIC FACIES ANALYSIS

This analysis focuses on the Paleocene-Eocene progradational systems, particularly the along-strike variability of the shelf-slope-basin-floor succession and the repetitive nature of shelf-edge failure. The interval is bound by two, regionally extensive marine flooding surfaces: (1) the Maastrichtian-Paleocene, and (2) the Early Oligocene (Figs 3 & 5). This interval comprises two major progradational sequences, separated by a composite middle Eocene erosion surface (Fig. 4). The thickness of the Paleocene to Early Oligocene sedimentary wedge ranges from 700 ms (*ca.* 965 m) in the north to <300 ms (*ca.* 415 m) in the south (Fig. 5ii). The terminology used in the following section is based on clinoform dip angles: shelf (<1°), slope (<6°), and basin-floor (sub-horizontal), which are contained within the larger, continental margin-scale system (see Patruno et al. 2015). The terms shelf-edge and mid-shelf deltas (see Porębski & Steel 2003) are here synonymous with shelf-edge and delta-scale/shoreline clinoforms (e.g. Patruno & Helland-Hansen 2018), respectively. An overview of the seismic facies, which essentially form the ‘building blocks’ of the (seismically imaged) margin, are outlined in Table 1. An index map has been included to navigate between figure locations (see Fig. 5). The boundaries of the so-called northern, central and southern areas of the dataset can be found in Figure 2. Below we describe twelve seismic facies in order of location along a clinothem, from shelf to basinfloor. Their amplitude/geometrical characteristics and interpreted depositional environments can be found in Tables 1 & 2.

Shelf

SF1: Landward-diverging, low- to high-amplitude, continuous reflections (shelf)

Description: SF1 is composed of parallel to landward diverging, sub-horizontal, very continuous reflections (Fig. 6). The packages are dominantly low-amplitude and are capped by high-amplitude continuous reflections, which we interpret as flooding surfaces (i.e. Maastrichtian-Paleocene and Early Oligocene). At the shelf-edge, reflections are truncated by basinward-dipping erosional surfaces. In their landward portions sub-horizontal reflections are either incised by low- (SF2) or high-amplitude (SF3) reflection packages, or merge with high-amplitude continuous packages (SF4) (Fig. 6 & 7).

Interpretation: SF1 dominates the shelf and are accordingly interpreted to represent a shallow-marine shelf environment. Variations in acoustic impedance represent variable interbedding of sandstone-mudstone units, and/or variations in the cementation state of an otherwise, relatively (lithologically) homogenous sequence.

SF2: Incised low-amplitude surfaces and low-amplitude fill (incised valley & fill)

Description: SF2 comprises a low-amplitude composite erosion surface that extends along-strike for up to 17.5 km and downslope for 14 km on the northern shelf. This surface consists of a series of smaller (2-6.5 km wide), NW-trending erosional surface (Fig. 7) that decrease in amplitude and relief (100 ms to below vertical resolution) toward the shelf-edge. Individual incisions are filled by up to 100 ms (ca. 140 m) thick packages of predominantly low-amplitude, low frequency, moderate continuity reflections that onlap the basal erosion surface.

Interpretation: The scale, topset location, and relative position of SF2 to the shelf-edge supports an interpretation of shelf-hosted incised valleys. Formation of these features may reflect prolonged periods of subaerial exposure, cannibalisation of the shelf, and sediment bypass to and beyond the shelf-edge. The overlying deposits likely represent background shelfal and/or estuarine mudstones, deposited during subsequent sea-level rise.

SF3: High-amplitude packages (fluvial channels)

Description: SF3 is represented by 50-1350 m wide belts of erosionally based, sinuous packages of high-amplitude reflections (Fig. 7). Like SF2, these features are restricted to the northern and central areas (Fig. 7). SF3 is concentrated along the flanks and at the base of the larger incisional events (SF2). Individual high-amplitude events are no more than two seismic cycles thick, thinning to one cycle towards the shelf-edge (c. 30 ms to vertical resolution).

Interpretation: The topset location of SF3, combined with its high-amplitude and sinuous plan-form support an interpretation of fluvial channels genetically related to the larger incised valleys (SF2). Figure 7iv suggests the sediment supply for the fluvial system may have been locally sourced from a salt-related high in the central to northern area of the shelf. More specifically SF2/3 trends parallel to the shelf, suggesting sediment transport orthogonal to the dominant NW-SE trend of the nearby shelf-edge.

SF4: Linear high-low amplitudes (beach ridges/strandplain)

Description: SF4 comprises a series of discrete, alternating high- and low-amplitudes features (Fig. 8). They have an irregular relief, with the high-amplitude anomalies generally forming mounded features (c. 20 ms TWT/ca. 28 m high) that are separated by low-amplitude depressions or horizontal reflections. In plan-view these high-/low-amplitude pairs form NW-trending, linear ridges and troughs that are 0.1-1 km wide and at least 28 km long (Fig. 8). Amplitude extractions show the ridges are parallel-to-subparallel to one another, are spaced 0.15-2.0 km, and occur in sets that are separated by subtle angular discordances (Fig. 8iii). A composite seismic line through a single high-amplitude ridge demonstrates the remarkable continuity of these features (Fig. 8ii), showing they migrate basinwards through time towards high-amplitude, continuous reflections (SF5). Within the same stratigraphic level as the linear features, a series low-amplitude, moderate to low frequency reflections are present. These are crescentic in map view, are up to 2.5 km long and 0.7 km wide and have the same NE trend as the linear features (Fig. 8iii/iv).

Interpretation: The SF4 ridges are oblique to the survey geometry, irregularly spaced, occur in clearly defined sets of subtly different trend, and show distinct amplitude patterns; this suggests these features are geological, rather than a seismic acquisition artefact/footprint (e.g. Marfurt et al. 1998) (Fig. 8). We therefore interpret the low-amplitude, convex-up features as sandstone-dominated beach ridges within a strandplain environment (see Otvos 2000; Jackson et al. 2010). The occurrence of beach ridges suggests a wave-dominated shelf, fed by along-shore transported sediment. We interpret the spatially related crescent-shaped features as back-barrier lagoons/bays; these have similar plan-form geometries to features observed in off-axis positions of the modern Pariba do Sul delta system (Fig. 8v).

SF5: Isolated high-amplitude continuous reflections (foreshore/upper shoreface)

Description: SF2, 3 and 4 are overlain by a set of high-amplitude, continuous, high-to-moderate frequency reflections that are restricted to the mid-shelf areas and capped by the early Oligocene flooding surface (Fig. 6i). They display the same NE trend as SF4, occurring in elongate belts (c. 28 km). They are, however, wider (up to 6 km) and thicker (up to c. 75 m), tapering towards the NE and SE. SF5 passes into low-amplitude/frequency, discontinuous seismic facies on the inner shelf.

Interpretation: SF5 shows many of the same characteristics as SF4 (i.e. the same NW-trending linear forms) suggesting a continuation of clastic shelf progradation. We therefore interpret SF5 to represent a foreshore to upper shoreface environment, with the high-amplitude bands potentially representing wide, sandstone-rich belts.

SF6: Parallel-oblique clinoforms (mid-shelf deltas)

Description: SF6 is composed of a series of parallel-oblique clinoforms (with some internal shingled and sigmoidal clinoforms) that downlap onto the shelfal deposits (SF1), and top lap or converge with semi-continuous, low-amplitude upper surfaces (Fig. 6). The clinoform foresets are 25-125 ms tall, up to 4250 m long, up to 7.8 km along-strike width, and thin from up to 350 ms (*c.* 480 m) in the northern area to 175 ms (*c.* 240) in the southern area. The clinoform downlap terminations trend approximately NE *c.* 058-238° in the northern area, shifting slightly to *c.* 042-222° further south. Clinoforms document >19 km of progradation, pinching-out just before the shelf-edge break (Fig.6). Internally the clinoforms have low-amplitude, low frequency, discontinuous to semi-continuous foresets that dip *c.* 2-3°, with topset convergence, and minor bottomset deposition/preservation. Clinoform trajectories are broadly flat. Above this prominent progradational sequence are several additional lower amplitude, progradational-to-retrogradationally stacked, parallel-oblique clinoform-bearing sequences, with contourite drift deposits (e.g. Rebesco et al. 2014) dominating the upper slope to basin-floor (Fig. 4i).

Interpretation: We interpret SF6 to represent progradation of a mid-shelf delta in water depths of up to 75 ms (*c.* 100 m), and re-establishment of the shelf after early Oligocene flooding. The variation in clinoform downlap orientation in the central part of the shelf is likely due to syn-depositional seabed deformation above a salt diapir (Fig. 6ii/iii). Overall, the shelf sequence suggests a primarily wave-dominated, strike-fed deltaic system, with minor fluvial input.

Outer-shelf to upper-slope

Mid-Eocene scarp

The outer-shelf to upper-slope is dominated by progradational-aggradational clinoform sets and related failure scarps, which vary in frequency and size along-strike. However, one main “composite” scarp is pervasive throughout the Paleocene-Eocene succession, cross-cutting multiple levels of stratigraphy, ranging in height from 600 ms (*c.* 825 m) in the NW to 50 ms (*c.* 69 m) in the SE, and dying out toward the south of the study area (Fig. 5iv & 10i). The scarp is gently arcuate in planform and trends broadly NE, dipping at ~6-7° and extending along-strike for 60 km. In section, the scarp is either linear (i.e. in the northern part of the study area; Fig. 9i, 12i) or highly irregular and scalloped (i.e. in the central part of the study area; Fig 9ii). Modica & Brush (2004) identified this regional middle Eocene scarp, showing it

extends along-strike for >250 km. Our work shows the interpretation can be extended south of the Sao Paulo transfer zone for another 50 km, terminating in the south of our study area.

SF7: Small-sigmoidal clinoforms (proto-shelf-edge deltas)

Description: SF7 consists of low-relief (typically 75-150 ms/ca. 105-205 m thick), low-angle (1-3°) clinoforms (Fig. 9). Cross-sectional geometries vary between sigmoidal to oblique-sigmoidal, with clinoforms downlapping underlying erosion surfaces (Fig. 9ii). The foresets are defined by low-amplitude, semi-continuous to discontinuous reflections. The clinoform heights periodically increase basinward, from <50ms to >150ms, before passing downdip into SF8 (see below). Clinoform topsets display both low and high amplitudes. Bottom sets vary along-strike, being characterised by either; (i) low-amplitude, discontinuous reflections; (ii) high-amplitude, isolated (c. <1 km along-strike), single-cycle reflections that are typically concentrated near the composite scarp; or (iii) thicker (c. 75 ms or 105 m), high-amplitude, chaotic reflections that, in many cases, are bound downdip by a terminal ramp (Fig. 9ii). Where preserved, SF7 clinoform-bearing sequences display falling to flat trajectories.

Interpretation: SF7 is only locally developed along up to 5 km strike-length of the shelf-edge to upper slope, typically being pounded in the middle Eocene scarp. We interpret SF7 likely represents the initial nucleation and progradation of shelf-edge deltas after formation of the irregular upper-slope scarp, an interpretation supported by its position on the upper slope and the fact it caps the middle Eocene scarp. Progradation of these deltas healed relief associated with the precursor shelf-edge/upper-slope failure.

SF8 & 9: Large-sigmoidal clinoforms (shelf-edge deltas)

Description: SF8 and 9 are dominated by clinoforms that are larger (ca. 200-500 ms or ca. 275-685 m tall) and steeper (ca. 5-6° dips) than those characterised by SF7. Clinoforms are sigmoidal to oblique-sigmoidal, extending along-strike for up to 20 km (Fig. 9i/ii). Amplitudes vary across the clinoform foresets: in central and southern areas, foresets are defined by continuous low- to moderate-amplitude reflections, whereas the bottomsets are low- to moderate-amplitude reflections of limited lateral continuity, whereas in the northern areas, foresets are seismically similar, but bottomsets have higher amplitudes and extend for up to 5 km along-strike (Fig. 9). The foresets in the central and northern area also contain isolated high-amplitude chaotic packages (SF9) that are c. 180-1650 m long, 75-200 m wide, and 25-50 ms (c. 35-70 m) thick. These packages trend parallel to clinoform dip and are concentrated directly downdip of SF7 or within the foresets of SF8. Many of the clinoform sets display offlap geometries and topset truncation, resulting in

limited topset preservation. We observed a consistent stacking pattern, with SF9 at the base of a sequence where reflection continuity is poorer, moving stratigraphically upward into SF8 where foresets and bottomset reflections become more continuous and dips decrease.

Interpretation: After initial nucleation of clinoforms at the head of the failure scarp (SF7), shelf-edge deltas (SF8), which increase in height basinward, effectively “heal” relief associated with the shelf-edge-upper-slope failure. Deltaic deposition increases the grade of the slope to a graded, stable equilibrium profile. The contorted packages (SF9) are interpreted as slumps which were likely sourced from failure of the shelf-edge deltas (e.g. Mayall et al. 1992; Porębski & Steel 2003).

Base of slope to proximal basin-floor

SF10: Chaotic-mounded reflections (mass-transport complexes)

Description: SF10 comprises a series of mounded packages that are located at the base of slope (Fig. 9). The packages are bound by high-amplitude reflections and are internally chaotic, displaying discontinuous low-amplitude reflections that onlap landward onto the composite erosion surfaces and thin basinward (Fig. 9). The high-amplitude top-surfaces have variable relief (c. 50 ms), related to ponding of clinoform bottomsets (SF8) in the depressions. The basal-surfaces are defined by continuous high-amplitude reflections that link updip to exactly the same stratigraphic surface defining the outer-shelf-to-upper shelf failure scarps (Fig. 10). Downdip, the basal surfaces may not be strata-concordant, but may instead display considerable relief associated with ramps (c. 50-125 ms) that cross-cut underlying stratigraphy (Fig. 10iii). Although the gross reflection character is chaotic, there are rare examples of fold-thrust systems (especially in downdip areas), and coherent blocks that are c. 100-600 m diameter and up to 150 ms (c. 205 m) thick. Similar to the shelf-slope system, the volume and frequency of chaotic deposits displays significant lateral variability: (i) the northern area comprises at least five discrete units, with a gross-thickness of up to 275 ms (c. 375 m), (ii) the central area contains two stacked units that together are up to 250 ms (c. 345 m) thick, and (iii) the central-southern comprises a single unit that is up to 75 ms (c. 105 m) thick and which pinches-out southward (Fig. 9, 12).

Interpretation: We interpret SF10 to represent mass-transport complexes (MTCs) emplaced by debris, slump or slide processes during shelf-margin failure (Dott 1963; Nardin 1979; Nemeč 1990). The high-amplitude basal surfaces likely represent kinematic boundary zones upon which the MTCs were transported (*sensu* Butler et al. 2016). The frontal ramps (Fig. 10iii), which forms due to erosion along the basal shear

surface, and the transported-blocks together provide kinematic indicators defining the overall transport direction of the MTC (c. 127°) (e.g. Frey-Martínez et al. 2006; Steventon et al. 2019).

SF11/12: High-amplitude continuous reflections (slope channels and toe-of-slope fans)

Description: SF11 and 12 comprises several high-amplitude, moderate- to low-frequency reflections located in the bottomsets of the shelf-edge deltas (Fig. 9). There are two main types of high-amplitude seismic facies: (i) SF11, which consists of discontinuous to semi-continuous high-amplitude reflections; and (ii) SF12, which comprises continuous, high-amplitude reflections (Fig. 9 & 11). Both seismic facies are offset by normal faults (Fig. 11i), The continuous bottomsets are up to 60 ms (c. 83 m) thick on the toe-of-slope and thin to vertical resolution on the lower slope. In strike-section, the moderate-amplitudes on the lower slope change basinward into high-amplitude bottomsets that have a central isochron thick that pinches-out towards its edges into low-amplitude reflections, thus defining a broad, lobate geometry (Fig. 11, B-B'). The discontinuous high-amplitude packages are stratigraphically higher than the lobate packages, and in strike section can be seen to incise into background (low-amplitude) facies (Fig. 11, A-A'). In map-view, SF11 trend subparallel to the shelf-edge, merging down-dip into SF12 (Fig. 11ii). The normal faulting was probably caused by underlying salt-withdrawal and display oblique NNE-SSW amplitude trends to the shelf-edge (Fig. 11).

Interpretation: The high-amplitude bottomset reflections (SF12) are interpreted to represent toe-of-slope lobes (fans), supplied by shelf-oblique submarine slope channels (SF11). A similar interpretation is presented for high-amplitude reflections located at the toe-of-slope of prograding shelf-edge deltas (Hadler-Jacobsen et al. 2005). Similar deposits have also been identified in the field (e.g. Steel et al. 2008).

SHELF-EDGE TRAJECTORY & ALONG-STRIKE VARIABILITY

The Paleocene-Eocene margin of the central Santos Basin was defined by a relatively low shelf-edge to basin-floor relief (see Hadler-Jacobsen et al. 2005), comprising a predominantly progradational to aggradational succession. Overall, the shelf-edge trajectory is complex in the north and becomes simpler towards the south with a single falling trend. In addition, the amount of shelf-edge progradation decreases southward (c. 5.5 km in the north, c. 3.0 km in the central, and c. 1 km in the southern area). In total, the succession has received a sediment flux (Q) of c. 68 km³ Myr⁻¹ over a c. 25 Myr time interval. Below we

compare the differences in clinoform trajectory and sediment flux between the northern, central and southern shelf-edge.

Northern shelf-edge

The northern shelf-edge has the most complex clinoform trajectory, which can be split into three main sequences (Fig. 13). The first (N1) is a falling/flat trajectory, with the shelf-edge delta building out from the updip margin of the underlying outer-shelf/shelf-edge failure scarp (Fig. 13, 9i). The foresets and bottomsets (up to 260 ms, *c.* 358 m) are dominated by shelf-edge delta slumps (SF9) and MTCs (SF10), indicating the margin was unstable at this time. Sequence 1 is separated from 2 by a package defining a distinct backstepping (825 m) of the shelf-edge (Fig. 13). Sequence 2 (N2) starts with a relatively short-lived falling/flat trajectory (Fig. 13, North-1), before changing to a rising trajectory. Shelf-edge delta slumps (SF9), which are confined to the clinoform foresets, are common in this interval, the bottomset succession is relatively thin (< 50 ms, *ca.* 69 m) when compared to N1 (Fig. 9i). Sequence 3 (N3) is a relatively long-lived falling/flat trajectory with notable offlap terminations (Fig. 9i). N3 is characterised by higher-amplitudes than N1 and N2, with slope channels (SF11) dominating the foresets and toe-of-slope fans (SF12) occurring in the bottomsets (up to 200 ms, *c.* 275 m). The northern area has a sediment flux of *c.* 28 km³ my⁻¹ and correlates to the area of maximum thickness on the slope (Fig. 5ii, *c.* 750 ms, *c.* 1000 m). The northern area shows correlation between sequence bottomset thickness and clinoform trajectory, with falling/flat trajectories having thicker, and rising trajectories thinner bottomsets (e.g. Steel & Olsen 2002).

Central shelf-edge

The central shelf-edge can be split into 2 main sequences and has a simpler trajectory than the northern shelf-edge (Fig. 13, 9ii). Both sequences are falling/flat. Sequence 1 (C1) is composed of shelf-edge delta clinoforms (SF7) that infill shelf-edge failure scarps, whereas sequence 2 (C2) is composed of larger shelf-edge delta (SF8) clinoforms (Fig. 9ii). The bottomsets of C1 are dominated by upper-slope shelf-edge delta slumps (SF9). C2 is thicker, with a mixture of toplap and offlap terminations at the shelf-edge, with downlap termination in the bottomsets (Fig. 9ii). Two slope-attached MTCs are present downdip of the central shelf-edge. However, it is unlikely these are related to the preserved clinoform trajectories, due to the fact they directly downlap onto the MTCs (Fig. 9i). Instead, these MTCs were likely related to clinoforms that collapsed and are thus no longer preserved. The central area has a lower sediment flux of *c.* 22 km³ Myr⁻¹ than the northern area and accordingly has a thinner slope succession (Fig. 5ii, up to 500 ms, *c.* 688m).

Although the central area is defined by flat/falling clinoform trajectories, only two MTCs are emplaced on the basin floor; other deep-water deposits, such as channels and lobes are absent.

Southern shelf-edge

The southern area has a simple, flat/falling trajectory. A single sequence is identified as most of the clinoform rollover points are difficult to identify and the margin is characterised by a ramp rather than clinoform geometry. The southern area has the lowest sediment flux of c. $18 \text{ km}^3 \text{ Myr}^{-1}$ (Fig. 5ii, up to 150ms, c. 205m).

DISCUSSION

The Paleocene-Eocene shelf-edge of the central Santos Basin demonstrates significant along-strike variability in terms of shelf-physiography and evolution, and the types of depositional systems occurring on the outer-shelf to basinfloor. Below we discuss: (i) along-strike variability at the local- and basin-scale, (ii) the driving mechanisms and style of shelf-edge collapse and subsequent accretion, and (iii) the controls on sediment partition and stratigraphic variability between the shelf-edge and deep-water.

Lateral variability in shelf-edge physiography

Local variability

The central Santos Basin system displays a range of lateral changes in stratigraphic architecture along the *ca.* 90-km-long shelf-edge (Fig. 5). These changes are either gradual (10s of km) or abrupt (<1 km), with the larger-scale lateral changes manifested as: (i) gross depositional sequence thinning from north to south, (ii) change in the rate of sediment supply, varying from $28 \text{ km}^3 \text{ Myr}^{-1}$ in the north to $18 \text{ km}^3 \text{ Myr}^{-1}$ in the south, (iii) changes in seismic facies along the shelf (incisional vs. conformable), shelf-edge (linear vs. complex failure scarps), slope (degradational vs. progradational), and base of slope (i.e. the relative proportions of MTCs to toe-of-slope fans), and (iv) shelf-edge trajectories, changing from complex in the north to simple in the south (Fig. 14). Hence, it is impossible to select a single, representative

depositional-dip-oriented section that captures this variability. Below we discuss the depositional and structural controls on this lateral variability.

Sedimentation

The shelf contains extensive NE-trending beach ridges, which are aligned sub-parallel to the shelf-edge (Fig. 5iv). These beach ridges record deposition within an extensive, wave-dominated coastal depositional system, likely characterised by a wave-dominated delta and flanking shorefaces. These covered large parts of the shelf and extended to the shelf-edge, particularly in the north (Fig. 5iv, 8). Wave-dominated shorelines and shelf-edge systems have the capacity to efficiently transfer sediment long distances along continental shelves (Snedden et al. 1988). Larger storm surges can incised into shoreface sequences redistributing sediment offshore by turbulent and mass-wasting processes (e.g. Rogers & Goodbred 2010). Shoreline and shelf systems also have the ability to transfer sediment down-dip from wave-dominated (Fig. 8) deltaic systems to the shelf-edge, and along-strike to shelf-slope conduits (e.g. incised valleys, canyons, gullies; Fig. 7) (Covault & Graham 2010; Hadler-Jacobsen et al. 2010; Peng et al. 2017). The observed variability may therefore be explained by differential sediment supply across the shelf-edge, with fluvial input in the northern area part of the present study area (and areas further north, outside of our dataset), with this sediment being redistributed along strike by alongshore processes (Fig. 1b). Hence, alongshore rather than fluvial point sources are thought to be the dominant process within this stratigraphic interval, with the northern area interpreted as a mixed wave-dominated fluvial-influenced system, and central/southern areas being more wave-dominated. Our interpretation of the style of shelf depositional system correlates with the observed shelf-edge and toe-of-slope deposition, with more sediment bypass in the north (MTCs and toe-of-slope fans) where fluvial input and sediment accumulation rate was highest, decreasing southwards as wave-action preferentially stored sediment along the shelf. This is consistent with other studies that demonstrate effective sediment bypass beyond the slope in fluvial-dominated systems, with wave-dominated systems more likely to promote storage on the shelf (Deibert et al. 2003; Dixon et al. 2012; Cosgrove et al. 2018).

Structure

Sediment supply, if high enough, can drive shelf-edge progradation even during rising sea-level or highstand conditions (Burgess & Hovius 1998). However, given the complex tectonic regime (transfer zones and salt-tectonics) of the central Santos Basin (Fig. 4, 5iv), it is likely that basin physiography also

influenced the observed lateral variability. Structures which may have influenced the inherited topography of the depositional system include; (i) the Albian Gap restricting sediment input south of the Sao Paulo transfer zone (Fig. 1), and (ii) spatial variability in subsidence rates during salt-wall rise and withdrawal (Fig. 5iv).

The Sao Paulo transfer zone marks the boundary between the Albian Gap, a very thick (up to 3 km), salt-related depocenter (Fig.1, see Jackson et al. 2015), and the present study area. One possible scenario is that the Albian Gap captured a significant amount of sediment delivered, along-strike, from high-sediment supply areas in the north of the Santos basin. This significant depocenter directly north of this study could have caused much of the southern Santos basin, including this study's area, to be sediment starved.

An alternative interpretation is that the Sao Paulo transfer zone in conjunction with active salt-tectonics created a basin physiography that preferentially focussed the north Santos basin sediment supply into the northern area of this study. Local salt-structures include an NNE-trending salt wall outboard of the shelf-slope break, and two stocks that underlie the northern and deeper southern parts of the shelf (Fig 5vi). We suggest salt tectonics, which was most active during the Late Cretaceous due to sediment loading, caused differential uplift of the shelf, and permitted overall subsidence in the downdip basin. Differential uplift is evidenced by localised incised-valley development along the northern shelf (Fig. 7); such valleys are absent in the south. Differential subsidence along the slope to toe-of-slope is demonstrated in the northern area where the supply axis of the shelf-edge delta has been fixed from approximately Coniacian-Maastrichtian times to the Early Oligocene (a ~50 Ma time-interval), while the southern area was sediment starved (Fig 12ii). After the Early Oligocene, this trend switched, with the southern area recording increased sediment input (Fig. 12, 14).

Basin-scale variability

In addition to the local variability, the shelf-edge also records basin-scale variability. North of the Ilha Grande transfer zone, outside of the study area (Fig. 1), the Paleocene-Eocene shelf-edge progrades in a similar manner, with the mid-Eocene scarp displaying a similar morphology (Berton & Vesely 2016). However, the shelf is more fluvially influenced than in this study, with multiple fluvial systems supplying sediment to Paleocene canyons and Eocene slope channel systems. This style of sediment delivery produces both mixed sand-mud and sand-rich (cf. Reading & Richards 1994) basin-floor fans, and sand-rich MTCs (Ebiwonjumi & Schwartz 2003; Berton & Vesely 2016; Vesely 2016). The Paleocene canyons are up to 300 m deep and are thought to be related to local uplift/relative sea-level fall, correlating with

the Maastrichtian-Paleocene (55-59 Ma) horizon mapped in this study (Cobbold et al. 2001; Modica & Brush 2004). However, the shelf still shows signs of being at least wave-influenced, with arcuate beach ridges imaged on the Eocene shelf (Dixon 2013). The area between the Ilha Grande and Sau Paulo transfer zones shows a similar pattern to the northern area of the basin, although large Paleocene canyons are not present (Modica & Brush 2004) (Fig. 1). Hadler-Jacobsen et al. (2010) argue this area was characterised by a predominantly wave-dominated shoreline during the Campanian-Maastrichtian, with shelf transport along-strike supplying canyons and slope channels, with large basin-floor fans at their terminus. We postulate this wave-dominated shoreline continues into the Paleocene-Eocene, forming the northern equivalent of the strandplain system identified here (Fig. 6i & 8). South of the Merluza transfer zone the sequence is condensed with no evidence of shelf-edge deltas (Modica & Brush 2004).

Model and mechanisms for collapse

Shelf-edge deltas are prone to oversteepening and periodic collapse (Nemec 1990). Previous studies of shelf-edge instability demonstrates the process: (i) is indiscriminate of deltaic regime, occurring in wave- (e.g. paleo-Orinoco Delta, Bowman & Johnson 2014), and fluvial-dominated (e.g. Cretaceous Spitsbergen, Nemec et al. 1988) systems, but being rarer in tide-influenced shelf-edge deltas (e.g. Cummings et al. 2006), (ii) varies significantly along-strike due to variations in allo- and autocyclic controls (e.g. Olariu & Steel 2009; Zhuo et al. 2018), (iii) is scale-independent, occurring from bed- (e.g. Flint et al. 2011; Hodgson et al. 2018), to system- (e.g. middle-Pliocene, Mississippi Canyon, Mayall et al. 1992), to basin-scale (e.g. this study), and (vi) shows predictable stacking patterns of degradational and later re-establishing sequences. Nevertheless, many shelf-edges are relatively stable and only infrequently experience minor instability in the form of soft sediment deformation on the shelf-edge, and turbidite/debrite deposition on the slope and basin-floor (Plink-Björklund et al. 2001; Mellere et al. 2002).

Many field and subsurface studies have proposed models for predicting stratigraphic and facies changes during shelf-edge accretion and collapse, capturing the role of relative sea-level, sediment supply, and inherited structure (e.g. Dixon et al. 2013; Peng et al. 2017; Gomis-Cartesio et al. 2018; Proust et al. 2018). Most of these models only capture 2D end-member or idealised-3D models of a sedimentary system, due to lack of subsurface data resolution and/or coverage, and/or limited exposure in the field. However, most of these models show a systematic pattern of margin development; i.e. an initial period progradation and then degradation is followed by a later re-establishment phase when relief associated with collapse of the shelf-edge/upper-slope is filled or “healed”. Studies focusing specifically on along-strike variability are forced to consider a basin in 3D, and identify that time-equivalent intervals along-strike can show vastly

differing patterns (e.g. Jones et al. 2015; Madof et al. 2016; Zhuo et al. 2018). These observations therefore suggest the cited 2D-models only have utility where they are related to a similar region of a depositional system (e.g. near the point source of a delta), and breakdown when used to predict changes along-strike. Here we build on these 2D examples by proposing a model capturing all aspects of basin variability, with focus on along-strike variations in sediment supply, considering high, moderate, and low Q end-members (Fig. 15).

Stage I: Pre-conditioning

Slope failure is primed and triggered by numerous factors (see Locat & Lee 2002; Sultan et al. 2004). In this study we interpret that slope failure is primed and ultimately triggered by slope oversteepening, which may be enhanced by a pore pressure increase and associated slope weakening during a period of rapid sediment accumulation. This may have occurred even during periods characterised by rising sea-level (i.e. rising trajectories) due to: (i) an increase in sedimentation rate during the middle Eocene, enhanced through renewed onshore uplift and increased sediment flux associated with the Paleocene-Eocene thermal maximum, a period of globally high temperatures, erosion, and sediment discharge to the global oceans (e.g. Self-Trail et al. 2017), (ii) a lack of conduits (e.g. submarine canyons) to allow sediment bypass, (iii) wave-dominated conditions on the shelf, which promote sediment storage at the shelf-edge, and (iv) a lack of evidence for sustained rising trajectories. These factors all suggest that, during periods of high shelfal accommodation, the shelf-edge prograded and aggraded (i.e. rising trajectory) to a critical slope angle that pre-conditioned the area to failure. Our interpretation is consistent with observations in the northern Santos Basin, where Eocene MTCs are thought to be sourced from highstand and transgressive units (Henriksen et al. 2011; Dixon 2013). This model for slope collapse (or at least preconditioning) is consistent with our observation that multiple failure events occurred in the high Q, northern and central area of this study, with the low Q southern part of the margin lacking slope (or ramp) failure and MTC emplacement.

We document multiple Eocene failure events in the Santos Basin, some of which are only locally developed. However, one event seems to be regionally extensive, being of broadly the coeval along ~300 km strike-length of the margin (e.g. Berton & Vesely 2016). Given this scarps significant size and, more specifically, strike extent of the related scarp, we suggest this event formed in response to a regional, allocyclic mechanism that acted at the basin-scale. We therefore suggest that a combination of a middle Eocene (40-43 Ma) eustatic sea-level fall (Modica & Brush 2004), and increased contourite current activity from Antarctic Bottom Water, which is thought to have entered the basin from the early Eocene (Barker et al. 1981; Duarte & Viana 2007), triggered the regional slope failure. Relative sea-level fall could have

increased the pore-pressure within shelf-edge and slope sediments (Posamentier & Kolla 2003), whereas contourite currents could have had a destabilising effect on an already weak slope (Rebesco et al. 2014). Together, these two mechanisms could have triggered regional failure of the middle Eocene shelf-edge and upper slope.

Stage 2: Degradation of the shelf-edge

Failure of the outer-shelf-to-shelf-edge is recorded as MTC(s) that were deposited on the basin-floor. The style of collapse varies across the shelf, with the high Q area in the north recording multiple larger shelf-edge failure events, the moderate Q area in the centre recording two large shelf-edge failure events (preserved as two stacked MTC; Fig. 9ii), and the low Q area in the south recording a condensed sequence at the base of slope. The area between the downdip part of the scarp and the onset of MTC deposition (which is essentially a toe-of-slope onlap surface) is a major sediment bypass surface (Fig. 9i & ii) (Stevenson et al. 2015).

Stage 3: Infill of scarp & re-establishment

Following shelf-edge failure, we observed two principal types of delta: (i) full re-establishment of shelf-edge scale clinoforms, and (ii) partial re-establishment of the upper slope with smaller scale clinoforms (SF7) transitioning into shelf-edge scale (SF8) (Fig. 9i & ii). Full re-establishment is observed in the high Q areas where the scars are linear. In these cases, we observed progradation of shelf-edge scale clinoforms (SF8), with delta-front slumps being deposited on the upper to middle slope. However, more commonly there is only partial re-establishment in both the high and moderate Q areas, where irregular scars in the upper slope are infilled by upper slope slumps (SF9) and small deltas (SF7). Similar depositional patterns are observed in the field. For example, in Cretaceous pro-delta sequences in eastern Spitsbergen, Norway, scarps are initially infilled by slump and debris flow deposits, followed by mud-rich turbidites that coarsen upwards (Nemec et al. 1988; Onderdonk & Midtkandal 2010). In the paleo-Orinoco pro-delta, upper slope facies successions demonstrate a mixture of relatively large shelf-edge failure (*c.* 50 m thick) with delta-front blocks, and smaller packages (m-scale) of thin-bedded turbidites and slumps (Bowman & Johnson 2014).

Once gradients on the upper slope stabilised, overlying deltaic deposits were able to re-establish, transitioning into shelf-edge scale clinothem packages. This suggests that, even after Stage 2, the shelf-

edge was still unstable, with re-establishment a process of smaller degradational events allowing infill and stabilisation of the irregular upper-slope morphology.

Stratigraphic prediction on degradational margins

Missing trajectories

In many examples in the north of our study area, flat/falling trajectories are correlated with shelf incision, offlapping geometries and high-amplitude reflections relating to toe-of-slope and basin-floor fan deposits. Hadler-Jacobsen et al. (2005) interprets the systems as a sediment over-filled margin, with larger basin-floor fans relating to flat/falling trajectories. MTCs are interpreted to be sourced from highstand/transgressive units (Henriksen et al. 2011; Dixon 2013). These interpretations agree with our own results, which show falling/flat trajectories are related to thicker bottomsets, rising trajectories are related to thinner bottomsets, and MTC represent remobilised rising trajectories.

Use of trajectory analysis has generally focused on examples that demonstrate the complete, or near complete, lateral and vertical migration of a break-in-slope. Generally rising, flat and falling trends can be used to predict delivery of sand-grade material to the basin floor, and hence predict reservoir presence (e.g. Steel & Olsen 2002). In shorelines, these migration pathways can be well-preserved, with modification through incision by later channels or canyons (e.g. Tesson et al. 2000). Similarly, many shelf-edges have little or only minor shelf-edge degradation (e.g. Johannessen & Steel 2005). However, on shelf-edges prone to multiple delta-front collapse phases (i.e. this study), preservation of shelf-edge trajectories is low. This poses difficulties in using trajectory methods including; incomplete preservation, diachroneity, and irregular upper slope gradients that may preferentially produce trajectories that do not represent conventional interpretations (e.g. falling trajectory = falling relative sea-level).

As shown in this study, degradational margins can include an under-representation of rising trajectories (due to remobilisation as MTCs) in the preserved shelf-edge trajectory. These “missing” trajectories may cause mis-interpretation of sediment partition from the shelf to basinfloor by either: (i) overpredicting falling/flat trajectories (Fig. 13), (ii) underpredicting rising trajectories and potential bias towards flat/falling trends that tend to be more stable, or (iii) underprediction of falling/flat trajectories in particular stratigraphic intervals, due to remobilisation during large-scale shelf-edge failure. Therefore, in addition to, flat, falling and rising trajectories, we should also consider missing trajectories (i.e. MTCs & smaller slumps) when analysing the stratigraphic development of degradation-prone shelf-edges.

Our interpretation suggest MTCs occurred mainly during times of rising trajectories contrary to many sequence stratigraphic models (e.g. Kolla & Perlmutter 1993) that would predict MTCs to occur during falling-stage to early lowstand systems tracts (falling trajectories). Our observations agree with other passive margin studies hypothesising MTCs to occur during both rising and falling relative sea-level (e.g. Maslin et al. 1998; Brothers et al. 2013). These results demonstrate the importance of understanding missing trajectories and the driving mechanisms behind shelf-edge failure, particularly if trying to apply conventional sequence stratigraphic concepts.

Lateral variability & non-uniqueness

In addition to predicting sediment partitioning in 2D, this study has shown the importance of along-strike variability in stratigraphic prediction for shelf-edge deltas, slope and toe-of-slope deposits. Yet, the concept of strike variability in sequence stratigraphy is not new. Martinsen & Helland-Hansen (1995) hypothesised how lateral variability in stacking patterns caused the use of systems tract-based models to become unreliable. More recently, Burgess & Prince (2015) use numerical models to show the potential for non-uniqueness, demonstrating that: (i) sequence bounding unconformities can be generated by both accommodation controls (i.e. relative sea-level fall) and variations in sediment transport rates, and (ii) similar shoreline/shelf-edge trajectories can be created with different accommodation and sediment transport rates. Similarly, maximum flooding/transgressive surfaces may not be present throughout a shelf-area, as demonstrated in moving hinge conceptual models, and do not always represent a single, coeval, correlative conformity (Madof et al. 2016).

The examples shown here from offshore Brazil are consistent with some of the predictions made above. For example, there is significant lateral variability in margin stacking pattern from north to south (Fig. 14). Without considering lateral changes or having access to three-dimensional data one could erroneously infer: (i) highstand (HST), falling-stage (FSST), lowstand (LST), and transgressive (TST) systems tracts in the northern area, (ii) FSST, LST and TST in the central area, and (iii) TST or HST in the southern area (Fig. 9, 12 & 14). In addition to stratal stacking patterns, this study shows lateral variability in key bounding surfaces. In particular, shelf incision and formation of an erosional surface in the north but not in south, possibly reflecting along-strike changes in differential subsidence rather than sediment supply and accumulation (see Burgess & Prince 2015). If we were to take a solely two-dimensional approach, we may erroneously relate incision of the northern shelf (Fig. 7) to a period of sea-level fall and lowstand. If so, we may interpret the erosional surface as a regionally developed sequence

boundary, and draw similarly incorrect conclusions regarding the nature, timing and distribution of sediment bypass beyond the shelf-edge to the slope and basin-floor. With our 3D control we can almost certainly say that this is a local not a regional unconformity, being the product of local incision. One surface that is extensive across the entire Santos Basin is the Early Oligocene flooding surface (Modica & Brush 2004), thought to be generated from eustatic sea-level rise. However, the resulting backstepping of the shelf is also approximately coeval with reorganisation of drainage away from the Santos and into the Campos basin, hence the flooding surface is most likely a product of both relative sea-level rise and decreased sediment flux.

The Paleocene-Eocene shelf-edge is an example of how sediment supply and structure may locally modify eustatic sea-level fluctuations and shows the importance of considering along-strike variability and degradational processes before applying a specific sequence-stratigraphic model. Regardless of how sophisticated sequence-stratigraphic models become, a basin-by-basin approach to understanding depositional systems is essential such that the likely role of allo- and autocyclic controls can be understood.

CONCLUSIONS

(i) The Paleocene-Eocene of the central Santos Basin is a wave-dominated shelf-edge, with minor fluvial influence. The shelf-edge is prone to failure and has produced a complex distribution of slope and toe-of-slope sedimentation. We build upon Modica & Brush (2004) basin-wide review to show the Paleocene-Eocene deltaic system, and potentially prospective toe-of-slope fans extends further south than previously thought.

(ii) The Paleocene-Eocene interval has shown to be prone to periodic shelf-edge collapse. We interpret the principle mechanism of repetitive failure to be related to oversteepening of the delta-front during periods of high sediment supply and shelfal accommodation. For the mid-Eocene scarp which represents a coeval catastrophic collapse from the central area of this study to the Cabo Frio High, we suggest a combination of eustatic sea-level fall and increased bottom-current activity.

(iii) We propose a 3D model for accretion styles on degradational shelf-edges, which incorporates lateral variability. The model distinguishes the changes in accretionary style and deposition from low to high sediment supplied shelf-edges, and can be split into three phases, Stage 1: pre-conditioning, Stage 2:

degradation and emplacement of the collapsed shelf-edge, and Stage 3: infilling of the upper-slope scarp and delta re-establishment.

(iv) Trajectory analysis has shown that falling/flat trajectories correlate with thicker bottomset and preserved rising trajectories correlate with thinner bottomsets, which is a generally accepted trend. However, we have also highlighted the importance of recognising MTC and smaller upper slope slumps as “missing” trajectories and incorporating these into interpretations of shelf-edge storage vs bypass.

(v) Lateral (along-strike) variability in shelf-edge, slope and toe-of-slope is the norm in both ancient and modern systems. We have demonstrated locally how over 10's km the style of shelf-edge accretion changes and interpret this variability to be predominantly caused by basin margin physiography and variations in sediment supply. Through confirmation with other Santos Basin studies we show this variability extends to the north and south, with variations in depocenter thicknesses, topset process regime and deep-water sedimentation.

(vi) This well constrained 3D example demonstrates the importance of building along-strike variability directly into predictive sequence stratigraphic, trajectory, and stratigraphic-forward models.

REFERENCES

Adams, E.W. & Schlager, W. 2000. Basic types of submarine slope curvature. *Journal of Sedimentary Research*, **70**, 814-828.

Barker, P.F., Carlson, R.L., Johnson, D.A., Cepek, P., Coulbourn, W., Gambôa, L.A., Hamilton, N., Melo, U., et al. 1981. Deep sea drilling project leg 72: Southwest Atlantic paleocirculation and Rio Grande Rise tectonics. *Geological Society of America Bulletin*, **92**, 294-309.

Berton, F. & Vesely, F.F. 2016. Stratigraphic evolution of Eocene clinoforms from northern Santos Basin, offshore Brazil: Evaluating controlling factors on shelf-margin growth and deep-water sedimentation. *Marine and Petroleum Geology*, **78**, 356-372.

Bowman, A.P. & Johnson, H.D. 2014. Storm-dominated shelf-edge delta successions in a high accommodation setting: The palaeo-Orinoco Delta (Mayaro Formation), Columbus Basin, South-East Trinidad. *Sedimentology*, **61**, 792-835.

Brothers, D.S., Luttrell, K.M. & Chaytor, J.D. 2013. Sea-level-induced seismicity and submarine landslide occurrence. *Geology*, **41**, 979-982.

Burgess, P.M. 2016. RESEARCH FOCUS: The future of the sequence stratigraphy paradigm: Dealing with a variable third dimension. *Geology*, **44**, 335-336.

Burgess, P.M. & Hovius, N. 1998. Rates of delta progradation during highstands: consequences for timing of deposition in deep-marine systems. *Journal of the Geological Society*, **155**, 217-222.

Burgess, P.M. & Prince, G.D. 2015. Non-unique stratal geometries: implications for sequence stratigraphic interpretations. *Basin Research*, **27**, 351-365.

Butler, R.W., Eggenhuisen, J.T., Haughton, P. & McCaffrey, W.D. 2016. Interpreting syndepositional sediment remobilization and deformation beneath submarine gravity flows; a kinematic boundary layer approach. *Journal of the Geological Society*, **173**, 46-58.

Carvajal, C., Steel, R. & Petter, A. 2009. Sediment supply: the main driver of shelf-margin growth. *Earth-Science Reviews*, **96**, 221-248.

Catuneanu, O. 2006. *Principles of sequence stratigraphy*. Elsevier.

Chang, H.K., Kowsmann, R.O., Figueiredo, A.M.F. & Bender, A. 1992. Tectonics and stratigraphy of the East Brazil Rift system: an overview. *Tectonophysics*, **213**, 97-138.

Clemson, J., Cartwright, J. & Booth, J. 1997. Structural segmentation and the influence of basement structure on the Namibian passive margin. *Journal of the Geological Society*, **154**, 477-482.

Cobbold, P.R., Meisling, K.E. & Mount, V.S. 2001. Reactivation of an obliquely rifted margin, Campos and Santos basins, southeastern Brazil. *AAPG Bulletin*, **85**, 1925-1944.

Cosgrove, G.I., Hodgson, D.M., Poyatos-Moré, M., Mountney, N.P. & McCaffrey, W.D. 2018. Filter Or Conveyor? Establishing Relationships Between Clinoform Rollover Trajectory, Sedimentary Process Regime, and Grain Character Within Intraself Clinothem, Offshore New Jersey, USA. *Journal of Sedimentary Research*, **88**, 917-941.

Covault, J.A. & Graham, S.A. 2010. Submarine fans at all sea-level stands: Tectono-morphologic and climatic controls on terrigenous sediment delivery to the deep sea. *Geology*, **38**, 939-942.

Cummings, D.I., Arnott, R.W.C. & Hart, B.S. 2006. Tidal signatures in a shelf-margin delta. *Geology*, **34**, 249-252.

Davison, I. 2007. Geology and tectonics of the South Atlantic Brazilian salt basins. *Geological Society, London, Special Publications*, **272**, 345-359.

Deibert, J., Benda, T., Løseth, T., Schellpeper, M. & Steel, R. 2003. Eocene clinoform growth in front of a storm-wave-dominated shelf, Central Basin, Spitsbergen: no significant sand delivery to deepwater areas. *Journal of Sedimentary Research*, **73**, 546-558.

Dixon, J., Steel, R. & Olariu, C. 2012. Shelf-edge delta regime as a predictor of deep-water deposition. *Journal of Sedimentary Research*, **82**, 681-687.

Dixon, J.F. 2013. Shelf-edge deltas: stratigraphic complexity and relationship to deep-water deposition.

Dixon, J.F., Steel, R.J. & Olariu, C. 2013. A model for cutting and healing of deltaic mouth bars at the shelf edge: mechanism for basin-margin accretion. *Journal of Sedimentary Research*, **83**, 284-299.

Dott, R. 1963. Dynamics of subaqueous gravity depositional processes. *AAPG Bulletin*, **47**, 104-128.

Duarte, C.S. & Viana, A.R. 2007. Santos Drift System: stratigraphic organization and implications for late Cenozoic palaeocirculation in the Santos Basin, SW Atlantic Ocean. *Geological Society, London, Special Publications*, **276**, 171-198.

Ebiwonjumi, F.R. & Schwartz, D. 2003. Eocene Depositional Model for the Brazil Santos Basin in the Vicinity of the BS-4—NE Discovery.

Flint, S., and Hodgson, D., Sprague, A., Brunt, R., Van der Merwe, W., Figueiredo, J., Pr lat, A., Box, D., et al. 2011. Depositional architecture and sequence stratigraphy of the Karoo basin floor to shelf edge succession, Laingsburg depocentre, South Africa. *Marine and Petroleum Geology*, **28**, 658-674.

Frey-Mart nez, J., Cartwright, J. & James, D. 2006. Frontally confined versus frontally emergent submarine landslides: a 3D seismic characterisation. *Marine and Petroleum Geology*, **23**, 585-604.

Galloway, W.E. 1998. Siliciclastic slope and base-of-slope depositional systems: component facies, stratigraphic architecture, and classification. *AAPG Bulletin*, **82**, 569-595.

Gomis-Cartesio, L.E., Poyatos-Mor , M., Hodgson, D.M. & Flint, S.S. 2018. Shelf-margin clinothem progradation, degradation and readjustment: Tanqua depocentre, Karoo Basin (South Africa). *Sedimentology*, **65**, 809-841.

Guerra, M.C. & Underhill, J.R. 2012. Role of halokinesis in controlling structural styles and sediment dispersal in the Santos Basin, offshore Brazil. *Geological Society, London, Special Publications*, **363**, 175-206.

Hadler-Jacobsen, F., Johannessen, E., Ashton, N., Henriksen, S., Johnson, S. & Kristensen, J. 2005. Submarine fan morphology and lithology distribution: a predictable function of sediment delivery, gross shelf-to-basin relief, slope gradient and basin topography. *Geological Society, London, Petroleum Geology Conference series*. Geological Society of London, 1121-1145.

Hadler-Jacobsen, F., Groth, A., Hearn, R.E., Liest l, F.M., Wood, L., Simo, T. & Rosen, N. 2010. Controls on and expressions of submarine fan genesis within a high accommodation margin setting, Santos Basin, Brazil—A high-resolution seismicstratigraphic and geomorphic case study. *Seismic Imaging of Depositional and Geomorphic Systems: Gulf Coast Section Society for Sedimentary Geology Foundation Annual Bob F. Perkins Research Conference Proceedings*, 572-615.

Hampson, G.J. 2016. Towards a sequence stratigraphic solution set for autogenic processes and allogenic controls: Upper Cretaceous strata, Book Cliffs, Utah, USA. *Journal of the Geological Society*, **173**, 817-836.

Haq, B.U., Hardenbol, J. & Vail, P.R. 1987. Chronology of fluctuating sea levels since the Triassic. *Science*, **235**, 1156-1167.

Helland-Hansen, W. & Gjelberg, J.G. 1994. Conceptual basis and variability in sequence stratigraphy: a different perspective. *Sedimentary Geology*, **92**, 31-52.

Helland-Hansen, W. & Martinsen, O.J. 1996. Shoreline trajectories and sequences: description of variable depositional-dip scenarios. *Journal of Sedimentary Research*, **66**.

Helland-Hansen, W. & Hampson, G. 2009. Trajectory analysis: concepts and applications. *Basin Research*, **21**, 454-483.

Henriksen, S., Helland-Hansen, W. & Bullimore, S. 2011. Relationships between shelf-edge trajectories and sediment dispersal along depositional dip and strike: a different approach to sequence stratigraphy. *Basin Research*, **23**, 3-21.

Hodgson, D., Browning, J., Miller, K., Hesselbo, S., Poyatos-Moré, M., Mountain, G. & Proust, J.-N. 2018. Sedimentology, stratigraphic context, and implications of Miocene intrashelf bottomset deposits, offshore New Jersey. *Geosphere*, **14**, 95-114.

Hunt, D. & Tucker, M.E. 1992. Stranded parasequences and the forced regressive wedge systems tract: deposition during base-level fall. *Sedimentary Geology*, **81**, 1-9, [http://doi.org/http://dx.doi.org/10.1016/0037-0738\(92\)90052-S](http://doi.org/http://dx.doi.org/10.1016/0037-0738(92)90052-S).

Jackson, C.A.-L. 2012. The initiation of submarine slope failure and the emplacement of mass transport complexes in salt-related minibasins: A three-dimensional seismic-reflection case study from the Santos Basin, offshore Brazil. *Geological Society of America Bulletin*, **124**, 746-761.

Jackson, C.A.-L., Jackson, M.P. & Hudec, M.R. 2015. Understanding the kinematics of salt-bearing passive margins: A critical test of competing hypotheses for the origin of the Albian Gap, Santos Basin, offshore Brazil. *Bulletin*, **127**, 1730-1751.

Jackson, C.A.-L., Grunhagen, H., Howell, J.A., Larsen, A.L., Andersson, A., Boen, F. & Groth, A. 2010. 3D seismic imaging of lower delta-plain beach ridges: lower Brent Group, northern North Sea. *Journal of the Geological Society*, **167**, 1225-1236.

Johannessen, E.P. & Steel, R.J. 2005. Shelf-margin clinoforms and prediction of deepwater sands. *Basin Research*, **17**, 521-550.

Jones, G.E., Hodgson, D.M. & Flint, S.S. 2015. Lateral variability in clinoform trajectory, process regime, and sediment dispersal patterns beyond the shelf-edge rollover in exhumed basin margin-scale clinoforms. *Basin Research*, **27**, 657-680.

Karner, G. & Gambôa, L. 2007. Timing and origin of the South Atlantic pre-salt sag basins and their capping evaporites. *Geological Society, London, Special Publications*, **285**, 15-35.

Karner, G.D. & Driscoll, N.W. 1999. Tectonic and stratigraphic development of the West African and eastern Brazilian Margins: insights from quantitative basin modelling. *Geological Society, London, Special Publications*, **153**, 11-40.

Kolla, V. & Perlmutter, M. 1993. Timing of turbidite sedimentation on the Mississippi Fan. *AAPG Bulletin*, **77**, 1129-1141.

Locat, J. & Lee, H.J. 2002. Submarine landslides: advances and challenges. *Canadian Geotechnical Journal*, **39**, 193-212.

Macedo, J. 1989. Evolução tectônica da Bacia de Santos e áreas continentais adjacentes. *Bol. Geoc. Petrobras*, **3**, 159-173.

Madof, A.S., Harris, A.D. & Connell, S.D. 2016. Nearshore along-strike variability: Is the concept of the systems tract unhinged? *Geology*, **44**, 315-318.

Marfurt, K.J., Scheet, R.M., Sharp, J.A. & Harper, M.G. 1998. Suppression of the acquisition footprint for seismic sequence attribute mapping. *Geophysics*, **63**, 1024-1035.

Martinsen, O.J. & Helland-Hansen, W. 1995. Strike variability of clastic depositional systems: Does it matter for sequence-stratigraphic analysis? *Geology*, **23**, 439-442.

Maslin, M., Mikkelsen, N., Vilela, C. & Haq, B. 1998. Sea-level—and gas-hydrate—controlled catastrophic sediment failures of the Amazon Fan. *Geology*, **26**, 1107-1110.

Mayall, M., Yeilding, C., Oldroyd, J., Pulham, A. & Sakurai, S. 1992. Facies in a Shelf-Edge Delta--An Example from the Subsurface of the Gulf of Mexico, Middle Pliocene, Mississippi Canyon, Block 109 (1). *AAPG Bulletin*, **76**, 435-448.

McMurray, L.S. & Gawthorpe, R.L. 2000. Along-strike variability of forced regressive deposits: late Quaternary, northern Peloponnesos, Greece. *Geological Society, London, Special Publications*, **172**, 363-377.

Meisling, K.E., Cobbold, P.R. & Mount, V.S. 2001. Segmentation of an obliquely rifted margin, Campos and Santos basins, southeastern Brazil. *AAPG Bulletin*, **85**, 1903-1924.

Mellere, D., Plink-Björklund, P. & Steel, R. 2002. Anatomy of shelf deltas at the edge of a prograding Eocene shelf margin, Spitsbergen. *Sedimentology*, **49**, 1181-1206.

Mitchum, R.M., Vail, P.R. & Sangree, J.B. 1977. Seismic stratigraphy and global changes of sea level: Part 6. Stratigraphic interpretation of seismic reflection patterns in depositional sequences: Section 2. Application of seismic reflection configuration to stratigraphic interpretation.

Modica, C.J. & Brush, E.R. 2004. Postrift sequence stratigraphy, paleogeography, and fill history of the deep-water Santos Basin, offshore southeast Brazil. *AAPG Bulletin*, **88**, 923-945.

Mohriak, W., Nemčok, M. & Enciso, G. 2008. South Atlantic divergent margin evolution: rift-border uplift and salt tectonics in the basins of SE Brazil. *Geological Society, London, Special Publications*, **294**, 365-398.

Moreira, J.L.P., Madeira, C., Gil, J. & Machado, M.P. 2007. bacia de Santos. *Boletim de Geociencias da PETROBRAS*, **15**, 531-549.

Muto, T., Steel, R.J. & Swenson, J.B. 2007. Autostratigraphy: a framework norm for genetic stratigraphy. *Journal of Sedimentary Research*, **77**, 2-12.

Nardin, T.R. 1979. A review of mass movement processes sediment and acoustic characteristics, and contrasts in slope and base-of-slope systems versus canyon-fan-basin floor systems.

Neal, J. & Abreu, V. 2009. Sequence stratigraphy hierarchy and the accommodation succession method. *Geology*, **37**, 779-782.

Neal, J.E., Abreu, V., Bohacs, K.M., Feldman, H.R. & Pederson, K.H. 2016. Accommodation succession ($\delta A/\delta S$) sequence stratigraphy: observational method, utility and insights into sequence boundary formation. *Journal of the Geological Society*, **173**, 803-816.

Nemec, W. 1990. Aspects of sediment movement on steep delta slopes. *Coarse-grained deltas*, **10**, 29-73.

Nemec, W., Steel, R., Gjelberg, J., Collinson, J., Prestholm, E. & Oxnevad, I. 1988. Anatomy of collapsed and re-established delta front in Lower Cretaceous of eastern Spitsbergen: gravitational sliding and sedimentation processes. *AAPG Bulletin*, **72**, 454-476.

Olariu, C. & Steel, R.J. 2009. Influence of point-source sediment-supply on modern shelf-slope morphology: implications for interpretation of ancient shelf margins. *Basin Research*, **21**, 484-501.

Onderdonk, N. & Midtkandal, I. 2010. Mechanisms of collapse of the Cretaceous Helvetiafjellet Formation at Kvalvågen, eastern Spitsbergen. *Marine and Petroleum Geology*, **27**, 2118-2140.

Otvos, E.G. 2000. Beach ridges—definitions and significance. *Geomorphology*, **32**, 83-108.

Partyka, G., Gridley, J. & Lopez, J. 1999. Interpretational applications of spectral decomposition in reservoir characterization. *The Leading Edge*, **18**, 353-360.

Patruno, S. & Helland-Hansen, W. 2018. Clinoform systems: Review and dynamic classification scheme for shorelines, subaqueous deltas, shelf edges and continental margins. *Earth-Science Reviews*.

Patruno, S., Hampson, G.J. & Jackson, C.A.L. 2015. Quantitative characterisation of deltaic and subaqueous clinoforms. *Earth-Science Reviews*, **142**, 79-119, <http://doi.org/https://doi.org/10.1016/j.earscirev.2015.01.004>.

Peng, Y., Steel, R.J. & Olariu, C. 2017. Transition from storm wave-dominated outer shelf to gullied upper slope: The mid-Pliocene Orinoco shelf margin, South Trinidad. *Sedimentology*, **64**, 1511-1539.

Plink-Björklund, P., Mellere, D. & Steel, R.J. 2001. Turbidite variability and architecture of sand-prone, deep-water slopes: Eocene clinoforms in the Central Basin, Spitsbergen. *Journal of Sedimentary Research*, **71**, 895-912.

Porebski, S.J. & Steel, R.J. 2003. Shelf-margin deltas: their stratigraphic significance and relation to deepwater sands. *Earth-Science Reviews*, **62**, 283-326.

Posamentier, H.W. & Kolla, V. 2003. Seismic geomorphology and stratigraphy of depositional elements in deep-water settings. *Journal of Sedimentary Research*, **73**, 367-388.

Posamentier, H.W., Allen, G.P., James, D.P. & Tesson, M. 1992. Forced regressions in a sequence stratigraphic framework: concepts, examples, and exploration significance (1). *AAPG Bulletin*, **76**, 1687-1709.

Prather, B.E., O'Byrne, C., Pirmez, C. & Sylvester, Z. 2017. Sediment partitioning, continental slopes and base-of-slope systems. *Basin Research*, **29**, 394-416.

Proust, J.-N., Pouderoux, H., Ando, H., Hesselbo, S.P., Hodgson, D.M., Lofi, J., Rabineau, M. & Sugarman, P.J. 2018. Facies architecture of Miocene subaqueous clinofacies of the New Jersey passive margin: Results from IODP-ICDP Expedition 313. *Geosphere*.

Reading, H.G. & Richards, M. 1994. Turbidite systems in deep-water basin margins classified by grain size and feeder system. *AAPG Bulletin*, **78**, 792-822.

Rebesco, M., Hernández-Molina, F.J., Van Rooij, D. & Wåhlin, A. 2014. Contourites and associated sediments controlled by deep-water circulation processes: state-of-the-art and future considerations. *Marine Geology*, **352**, 111-154.

Rogers, K.G. & Goodbred, S.L. 2010. Mass failures associated with the passage of a large tropical cyclone over the Swatch of No Ground submarine canyon (Bay of Bengal). *Geology*, **38**, 1051-1054.

Ross, W., Halliwell, B., May, J., Watts, D. & Syvitski, J. 1994. Slope readjustment: a new model for the development of submarine fans and aprons. *Geology*, **22**, 511-514.

Saenz, C.T., Hackspacher, P., Neto, J.H., Iunes, P., Guedes, S., Ribeiro, L. & Paulo, S. 2003. Recognition of Cretaceous, Paleocene, and Neogene tectonic reactivation through apatite fission-track analysis in Precambrian areas of southeast Brazil: association with the opening of the south Atlantic Ocean. *Journal of South American Earth Sciences*, **15**, 765-774.

Self-Trail, J.M., Robinson, M.M., Bralower, T.J., Sessa, J.A., Hajek, E.A., Kump, L.R., Trampush, S.M., Willard, D.A., *et al.* 2017. Shallow marine response to global climate change during the Paleocene-Eocene Thermal Maximum, Salisbury Embayment, USA. *Paleoceanography*, **32**, 710-728.

Snedden, J.W., Nummedal, D. & Amos, A.F. 1988. Storm-and fairweather combined flow on the central Texas continental shelf. *Journal of Sedimentary Research*, **58**, 580-595.

Steel, R. & Olsen, T. 2002. Clinoforms, clinoform trajectories and deepwater sands.

Steel, R.J., Carvajal, C., Petter, A.L., Uroza, C., Hampson, G., Burgess, P. & Dalrymple, R. 2008. Shelf and shelf-margin growth in scenarios of rising and falling sea level. *Recent advances in models of siliciclastic shallow-marine stratigraphy*, **90**, 47e71.

Stevenson, C.J., Jackson, C.A.-L., Hodgson, D.M., Hubbard, S.M. & Eggenhuisen, J.T. 2015. Deep-water sediment bypass. *Journal of Sedimentary Research*, **85**, 1058-1081.

Steventon, M.J., Jackson, C.A.L., Hodgson, D.M. & Johnson, H.D. 2019. Strain analysis of a seismically-imaged mass-transport complex (MTC), offshore Uruguay. *Basin Research*.

Sultan, N., Cochonat, P., Canals, M., Cattaneo, A., Dennielou, B., Hafliðason, H., Laberg, J., Long, D., *et al.* 2004. Triggering mechanisms of slope instability processes and sediment failures on continental margins: a geotechnical approach. *Marine Geology*, **213**, 291-321.

Tesson, M., Posamentier, H.W. & Gensous, B. 2000. Stratigraphic organization of late pleistocene deposits of the western part of the Golfe du Lion shelf (Languedoc shelf), Western Mediterranean Sea, using high-resolution seismic and core data. *AAPG Bulletin*, **84**, 119-150.

Torsvik, T.H., Rouse, S., Labails, C. & Smethurst, M.A. 2009. A new scheme for the opening of the South Atlantic Ocean and the dissection of an Aptian salt basin. *Geophysical Journal International*, **177**, 1315-1333.

Vail, P.R., Mitchum Jr, R. & Thompson III, S. 1977. Seismic stratigraphy and global changes of sea level: Part 3. Relative changes of sea level from Coastal Onlap: section 2. Application of seismic reflection Configuration to Stratigraphic Interpretation.

Van Bemmelen, P.P. & Pepper, R.E. 2000. Seismic signal processing method and apparatus for generating a cube of variance values. Google Patents.

Van Wagoner, J.C., Mitchum, R., Campion, K. & Rahmanian, V. 1990. Siliciclastic sequence stratigraphy in well logs, cores, and outcrops: concepts for high-resolution correlation of time and facies.

Vesely, F.F. 2016. Seismic expression of depositional elements associated with a strongly progradational shelf margin: northern Santos Basin, southeastern Brazil. *Brazilian Journal of Geology*, **46**, 585-603.

Weimer, P. 1989. Sequence stratigraphy of the Mississippi Fan (Plio-Pleistocene), Gulf of Mexico. *Geo-Marine Letters*, **9**, 185-272.

Williams, B.G. & Hubbard, R.J. 1984. Seismic stratigraphic framework and depositional sequences in the Santos Basin, Brazil. *Marine and Petroleum Geology*, **1**, 90-104.

Zhuo, H., Wang, Y., Sun, Z., Wang, Y., Xu, Q., Hou, P., Wang, X., Zhao, Z., et al. 2018. Along-strike variability in shelf-margin morphology and accretion pattern: An example from the northern margin of the South China Sea. *Basin Research*.

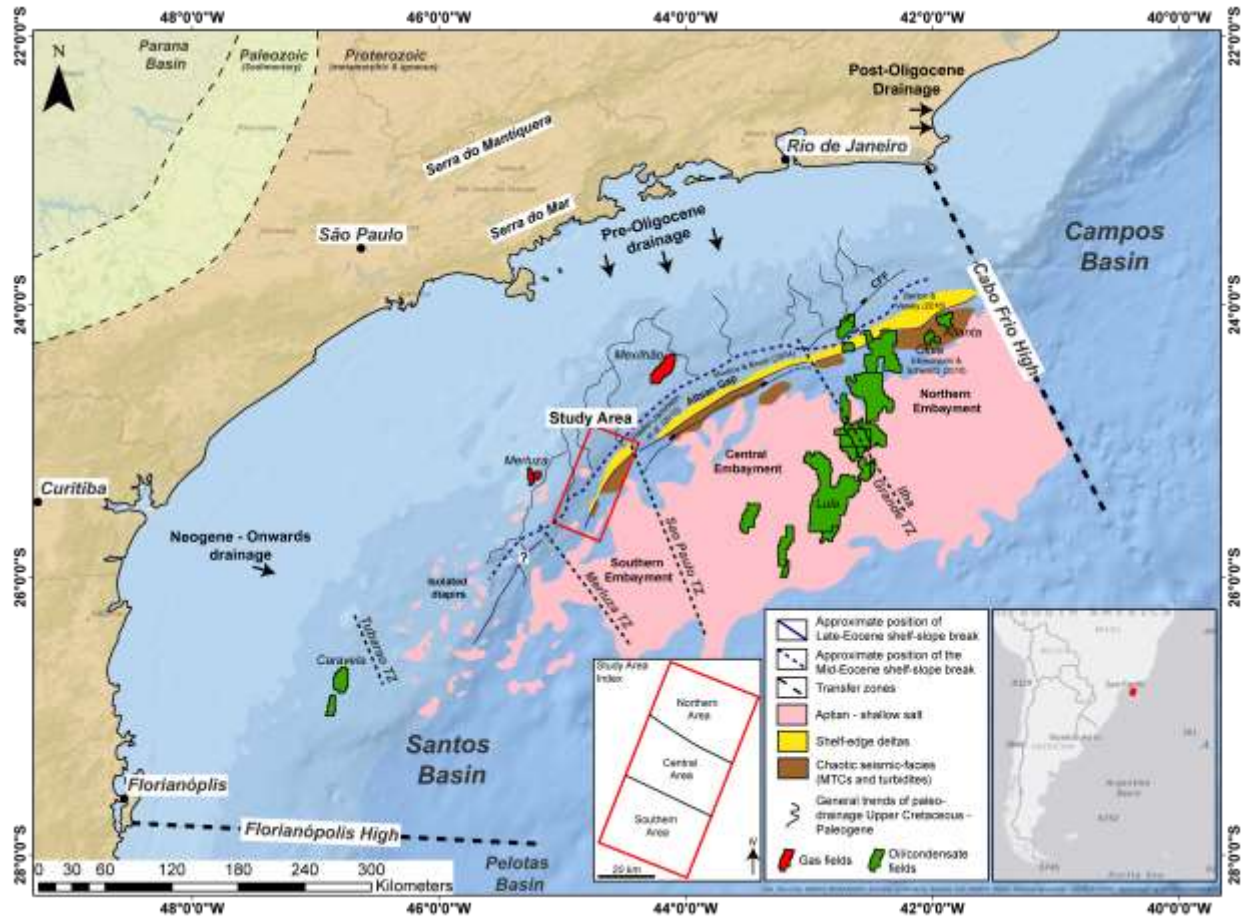


Figure 2: Location map of the Santos Basin, study area in the red box, with gross-depositional elements from the mid-Eocene modified from (Modica & Brush 2004). NE-SW depositional trend of the Eocene shelf-edge deltas and related MTCs and turbidites. Both the Atlanta and Oliva fields sit within the Eocene base-of-slope. Note study area index map depicting, northern, central and southern areas.

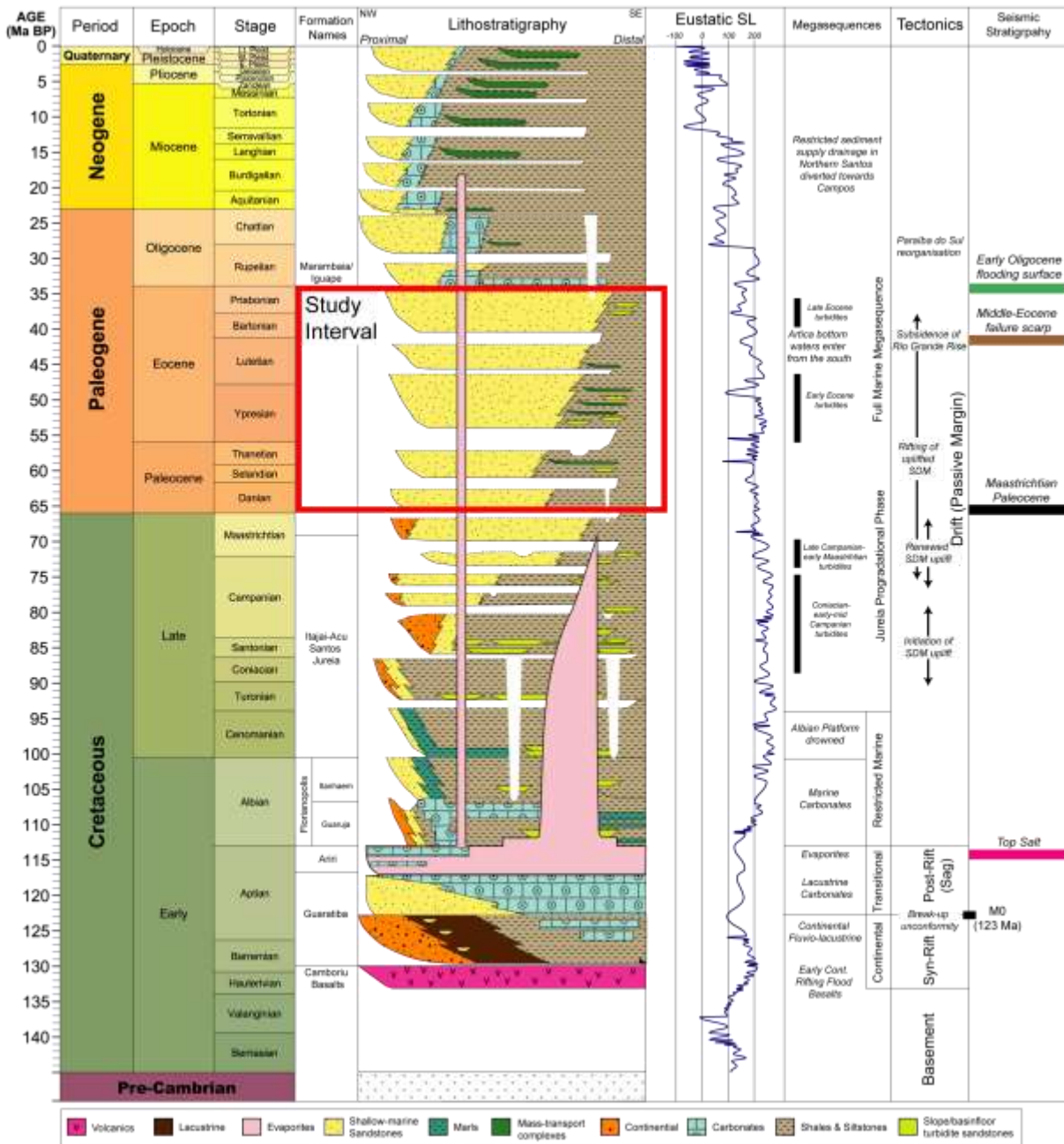


Figure 3: Tectono-stratigraphy of the Santos Basin collated from (Meisling et al. 2001; Modica & Brush 2004; Duarte & Viana 2007; Moreira et al. 2007; Jackson 2012) and observations from this study's dataset. Global sea-level curve from (Haq et al. 1987). SDM = Serra do Mar mountain range.

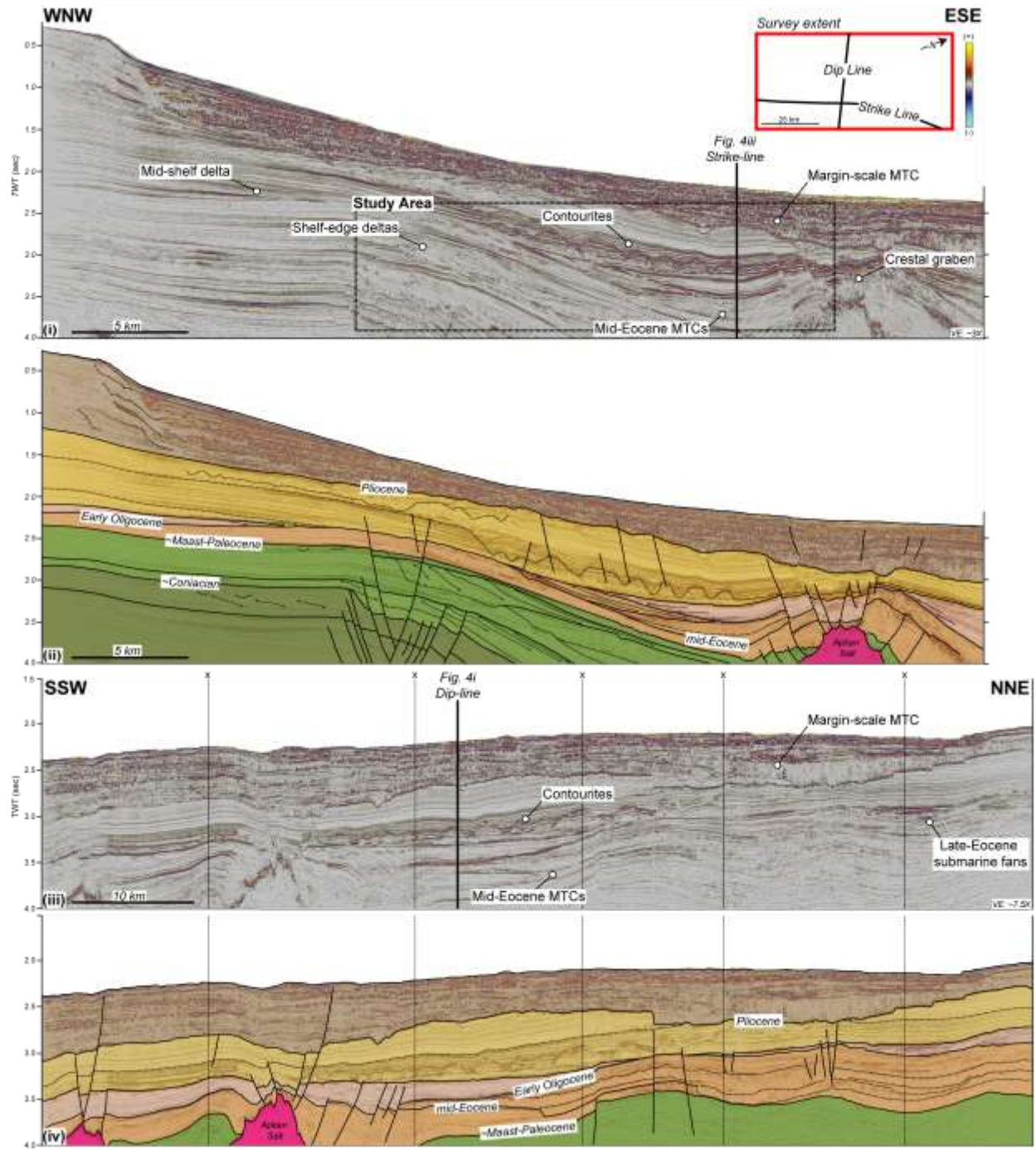


Figure 4: (i) Dip-oriented seismic section within the central area of the survey outlining shelf-edge deltas of the Jureia progradational phase and related slope-attached MTC, (ii) dip-oriented geosection, (iii) strike-oriented seismic section through the late-Cretaceous to Eocene base of slope sequence (iv) strike-oriented geosection. Note thinning of the Maastrichtian-Paleocene to Early Oligocene to the south. Stratigraphic ages are estimated from Modica & Brush (2004); Davison (2007); Berton & Vesely (2016).

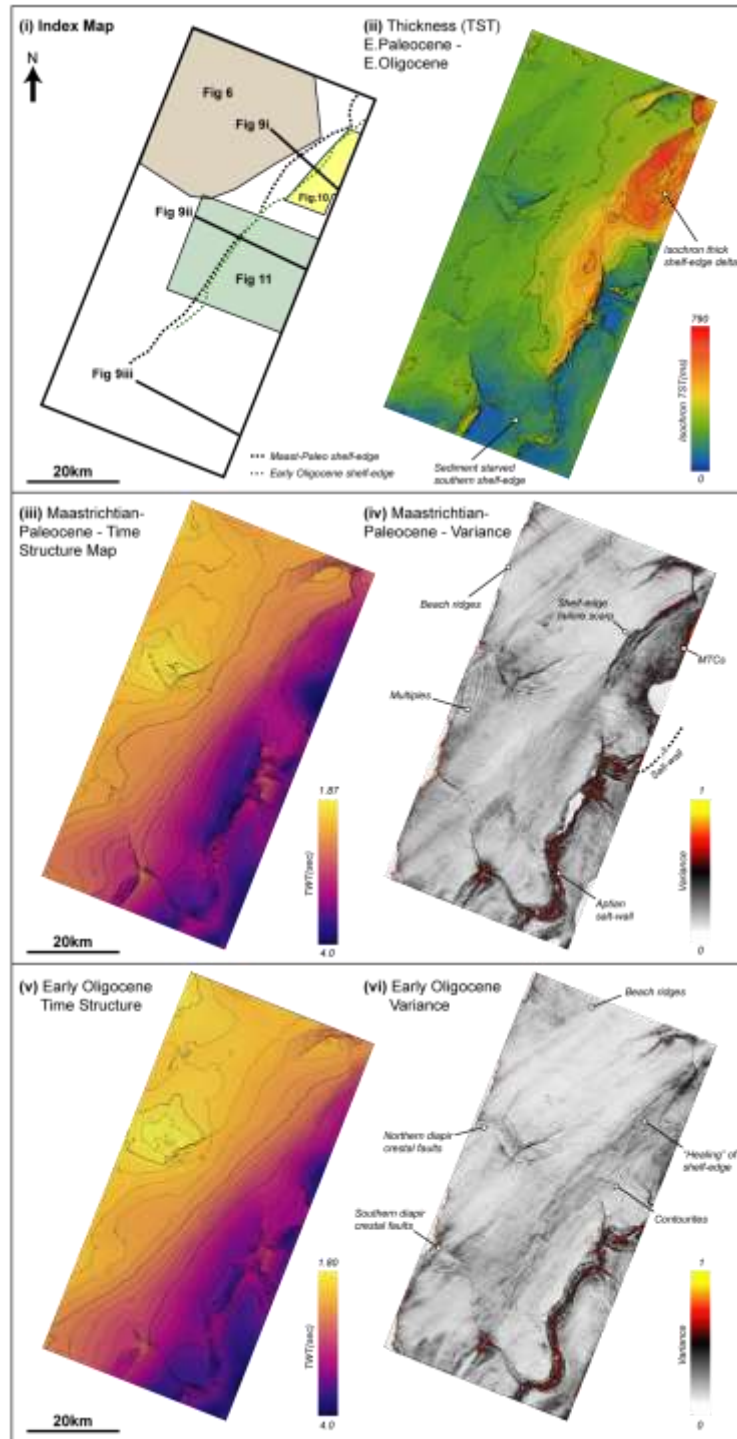


Figure 5: (i) Index map with locations of Maastrichtian -Paleocene and Early Oligocene shelf-slope breaks, (ii) time-thickness map (isochron, TST = true stratigraphic thickness) between the Maastrichtian-Paleocene and Early Oligocene, note thickness decrease at the shelf-edge and slope from north to south, (iii) Maastrichtian-Paleocene time-structure map, (iv) variance extraction of the Maastrichtian-Paleocene showing significant shelf-edge failure scarp in the north, an Aptian salt wall to the south and an isolated diapir along with linear sets (see Fig.7) on the shelf (v) Early Oligocene time-structure map, (vi) variance extraction of the Early Oligocene, note shelf-edge failure scarp has been infilled by progradation of subsequent shelf-edge deltas.

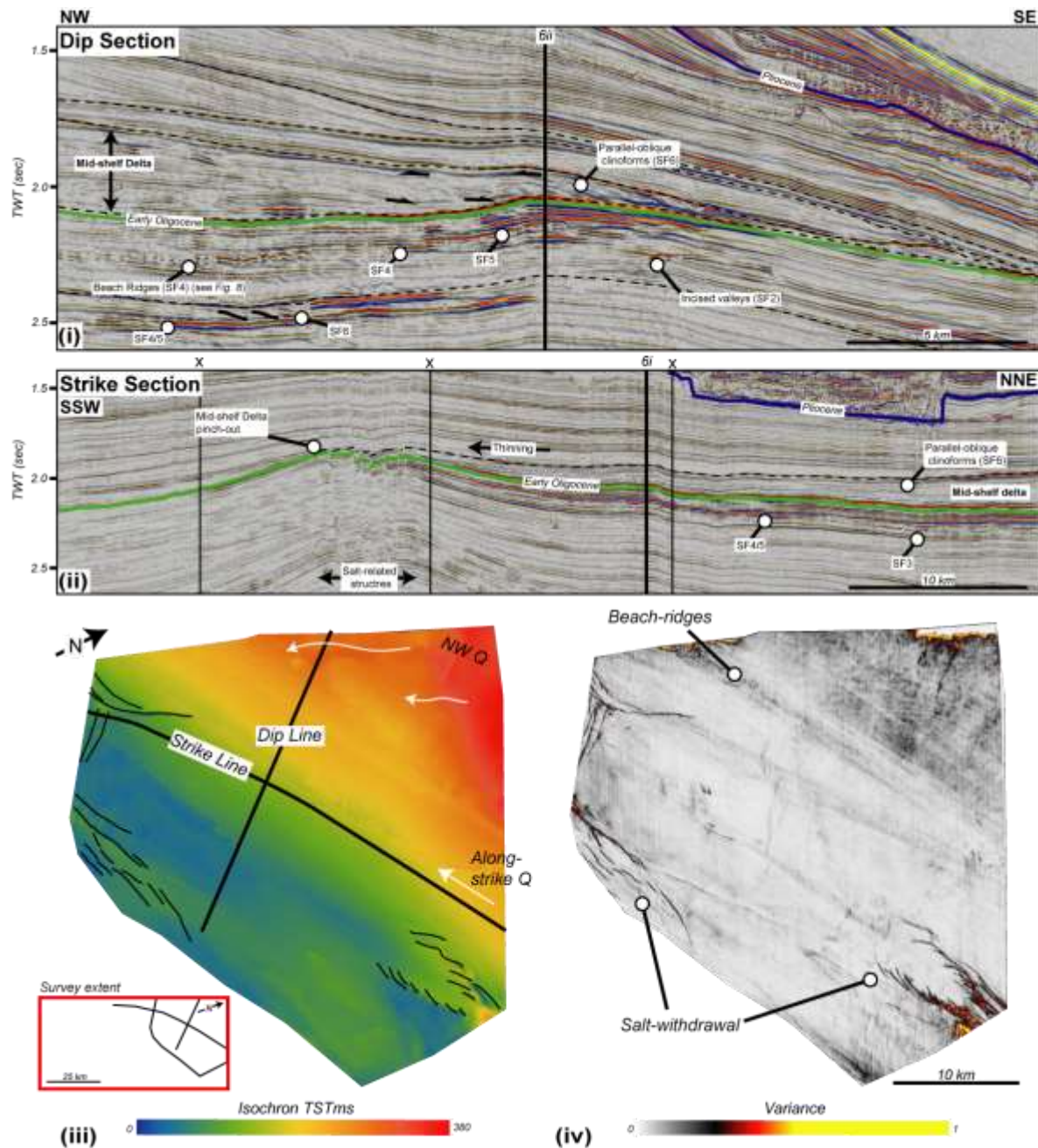


Figure 6: Northern shelf, (i) dip-oriented seismic section through the northern shelf highlighting sequences of mid-shelf deltas (SF6), related beach-ridges (SF4), and incised valley fill (SF2), (ii) strike-oriented seismic section, note thinning of the sequence towards the salt-related structural high, (iii) time-thickness map (isochron, TST = true stratigraphic thickness) between the toplap and downlap surfaces in the dip-oriented section, note significant thinning towards the shelf-edge, (iv) variance extraction of the downlap surface, highlighting salt-related structures and beach-ridges (SF4).

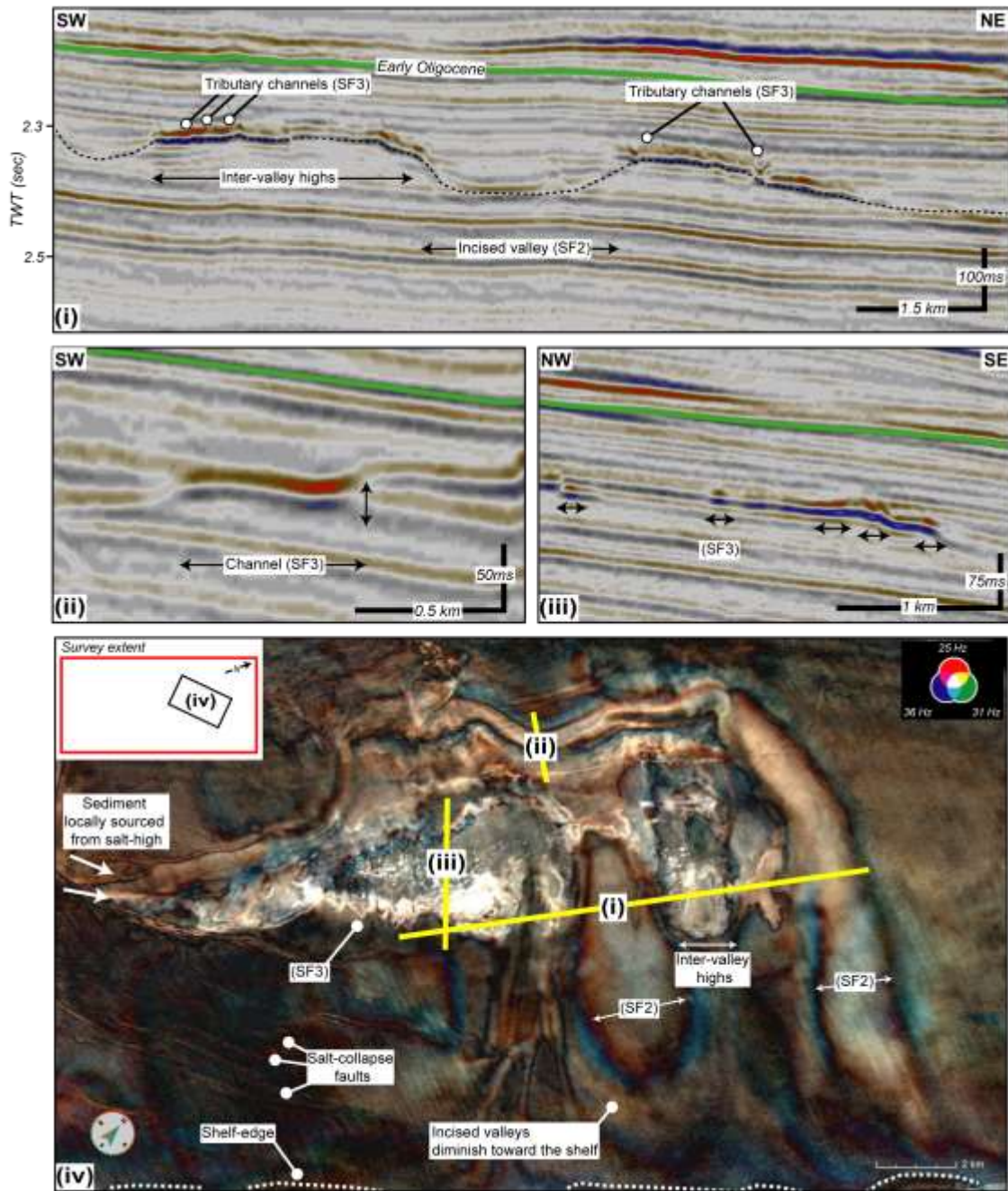


Figure 7: Beach-ridges/strandplain seismic facies, (i) dip-oriented seismic section through beach ridges and swales (SF4) note alternating high and low amplitudes, (ii) strike-section, note high-amplitude and continuity of the ridge, (iii) RMS amplitude and spectral decomposition extractions through the ridges and swales, note linear plan-view form, discordances between sets and crescent shaped reflections interpreted as lagoons, (iv) spectral decomposition extraction 50ms below the Early Oligocene showing a distributary channel system incising into the strandplain, (v) modern-day Pariba do Sul strandplain/beach ridge system (source Google Earth), inset map showing modern day river in flood with along-strike sediment transport (source NASA Earth Observatory), note scales similar to ancient depositional system shown in this study.

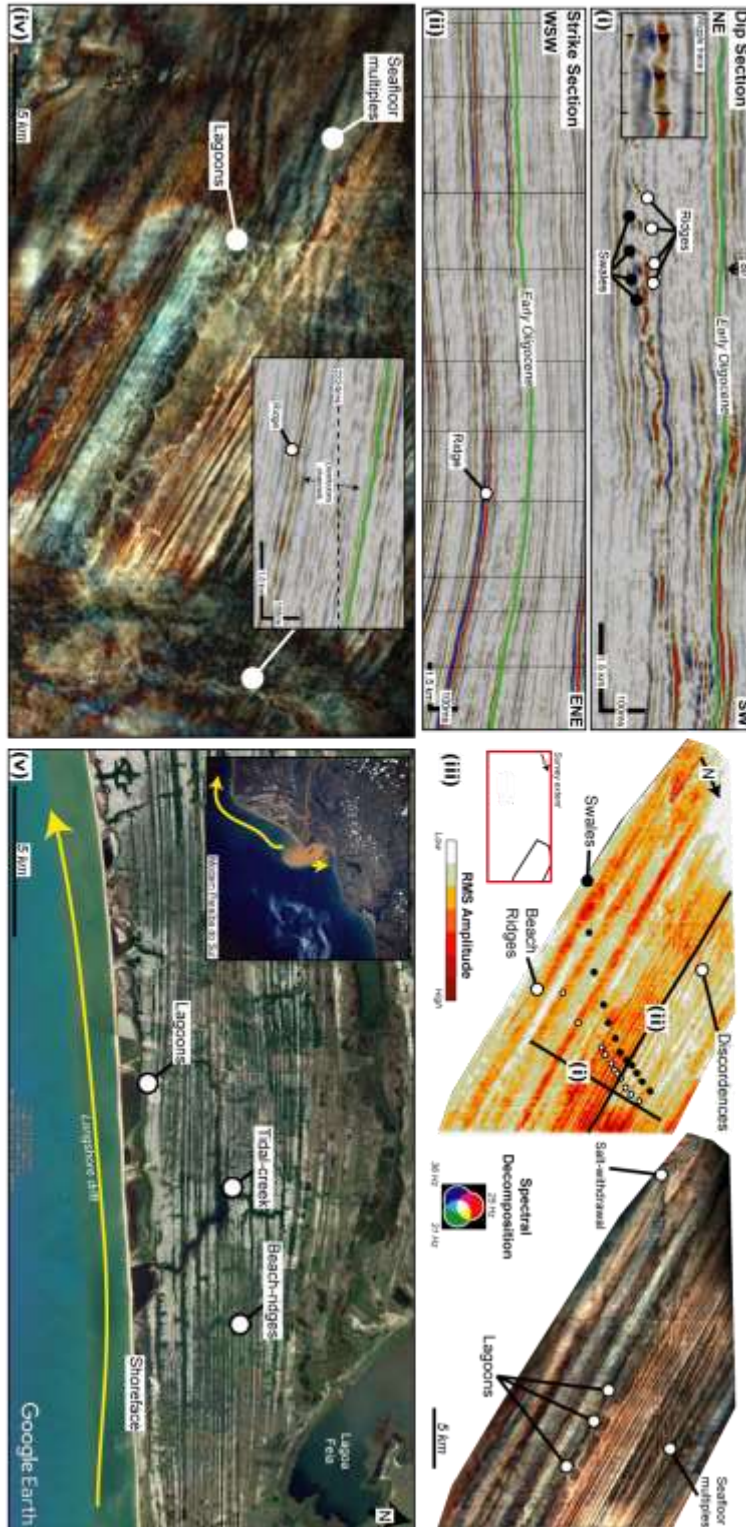


Figure 8: (i/ii) Seismic sections of the relationship between incised valleys (SF2) and related distributary channels (SF3), (iv) spectral decomposition extraction from 150ms below the Early Oligocene, showing the spatial relationship between incised valleys, inter-valley areas and distributary channels.

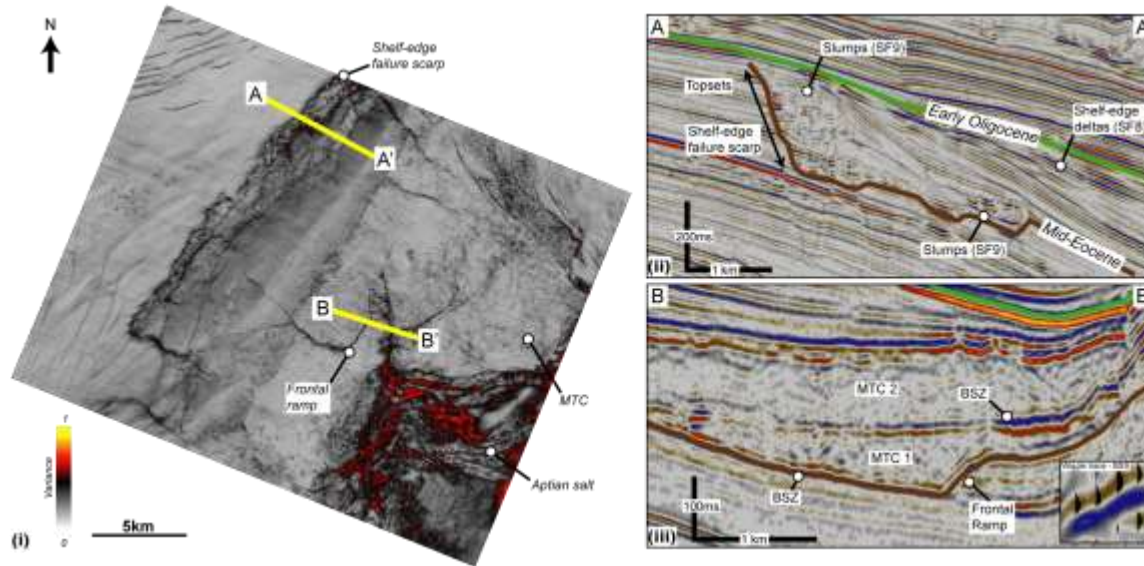


Figure 10: MTCs in the central region of the study area, (i) variance extraction from the mid-Eocene failure scarp, demonstrating that the scarp is a zone of deformation rather than a single plane, (ii) dip seismic section through the scarp zone, note minor slumping on the upper slope (SF9), (iii) dip seismic section through 2 seismically imaged MTCs (SF10), note high-amplitude basal-shear zones (BSZ), a frontal-ramp, and the internal chaotic seismic texture of the MTCs.

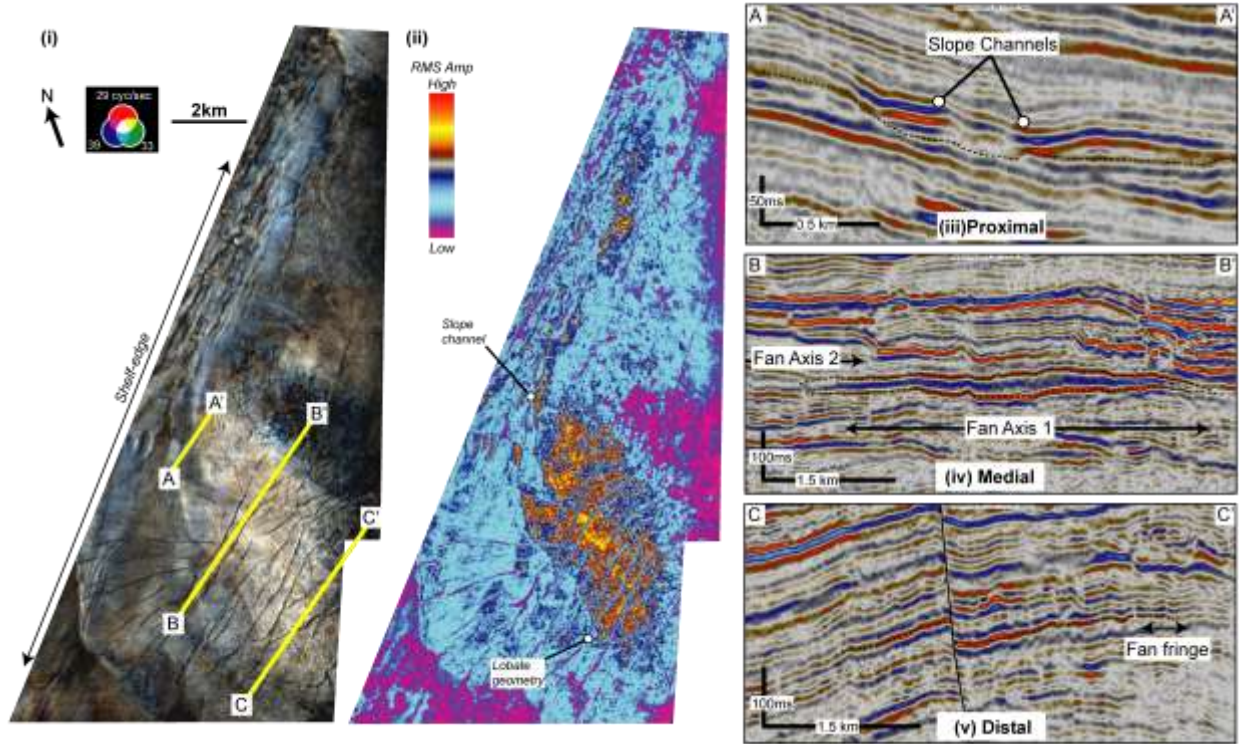


Figure 11: Toe-of-slope fan system in northern region of the study area, (i/ii) spectral decomposition and RMS amplitude extraction from clinoform labelled in Fig. 9i, note the elongate lobate geometry (SF12) at the toe-of-slope manifested as a high-amplitude response in a background of low-amplitudes and along-strike amplitudes on the slope, (iii) A-A' proximal strike seismic section showing isolated high amplitude reflections interpreted as slope channels (SF11), (iv) B-B' medial strike seismic section through the central axis of the fan, note isochron thick in the centre thinning towards the fan fringes, (v) C-C' distal strike seismic section with salt-related normal faulting.

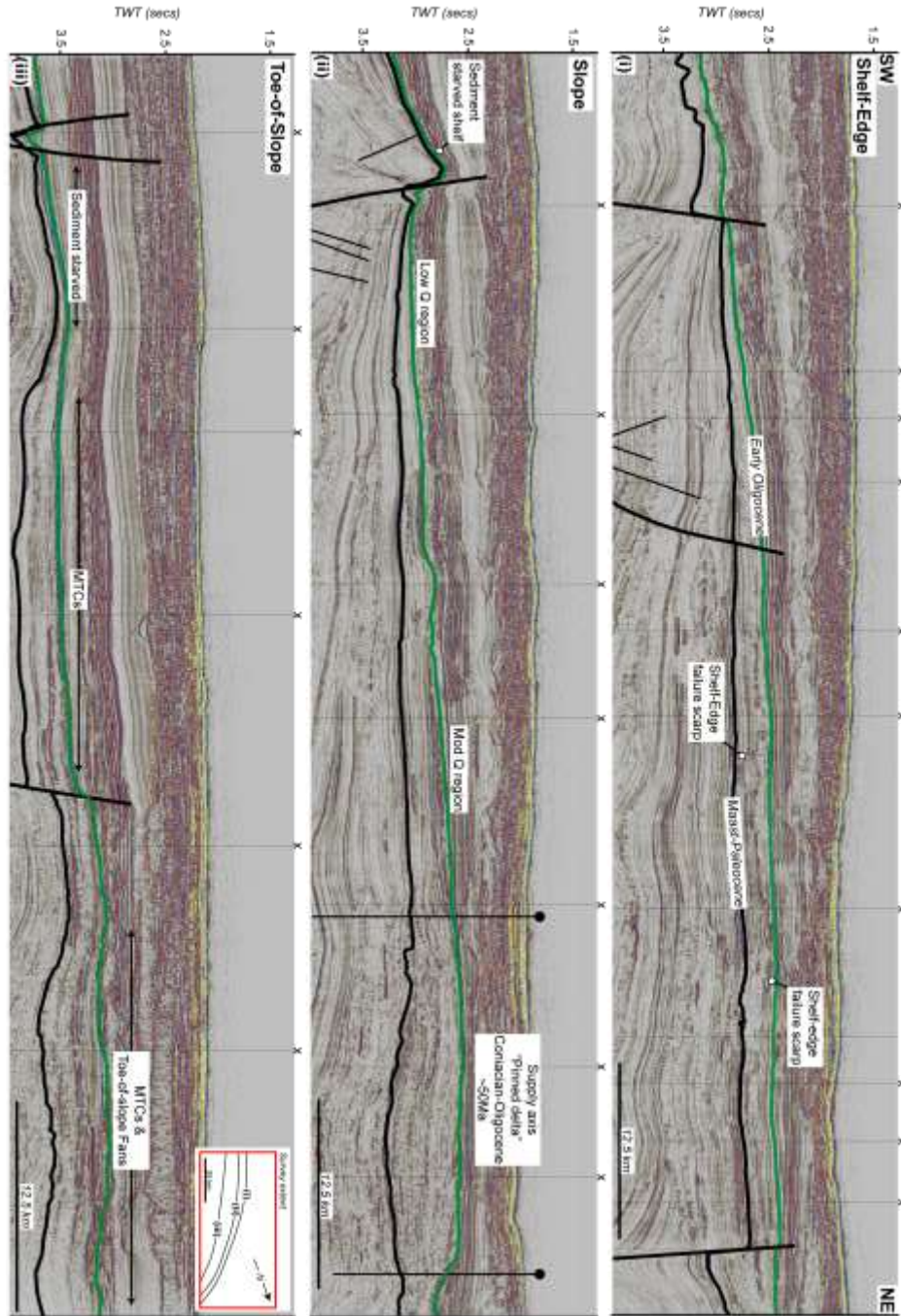


Figure 12: Strike variability of the Maastrichtian-Paleocene to Early Oligocene shelf-edge, note time-thickness decrease in all seismic sections from north (high Q) to south (low Q), (i) shelf-edge strike seismic section with failure scarps appearing as irregular incisional features, (ii) slope strike section recording significant deltaic input in the north where the sediment supply axis has remained fixed through-out the time-interval, with significant stratigraphic thinning towards the south, (iii) toe-of-slope seismic strike section with toe-of-slope fans (SF12) and MTCs (SF10) dominant in the north, MTCs dominant in the central area, and a condensed sequence recorded in the south.

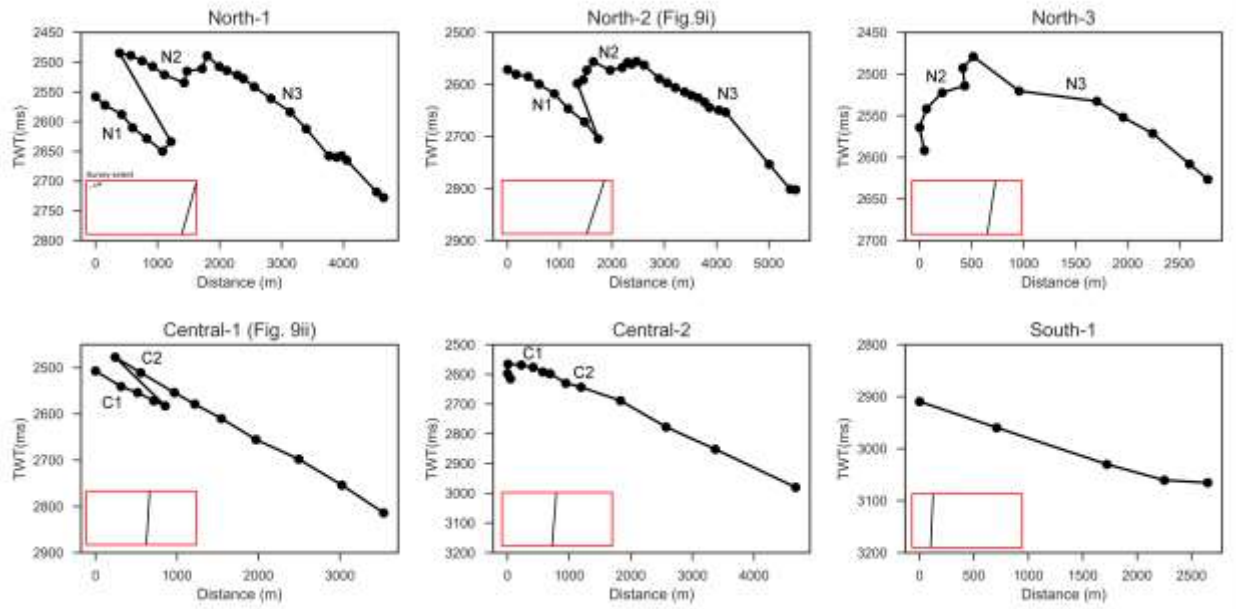


Figure 13: Clinoform trajectories from mid-Eocene to Early Oligocene demonstrate a complex signature in the north with rising, falling and flat trajectories, in the central area the shelf-edge is characterised by a predominantly falling trajectory, and in the south the shelf-edge is either falling or clinoform rollover points are absent/below seismic resolution. North-2 and Central-1 represent the northern and central dip-sections in Fig.9, others can be found in the supplementary material.

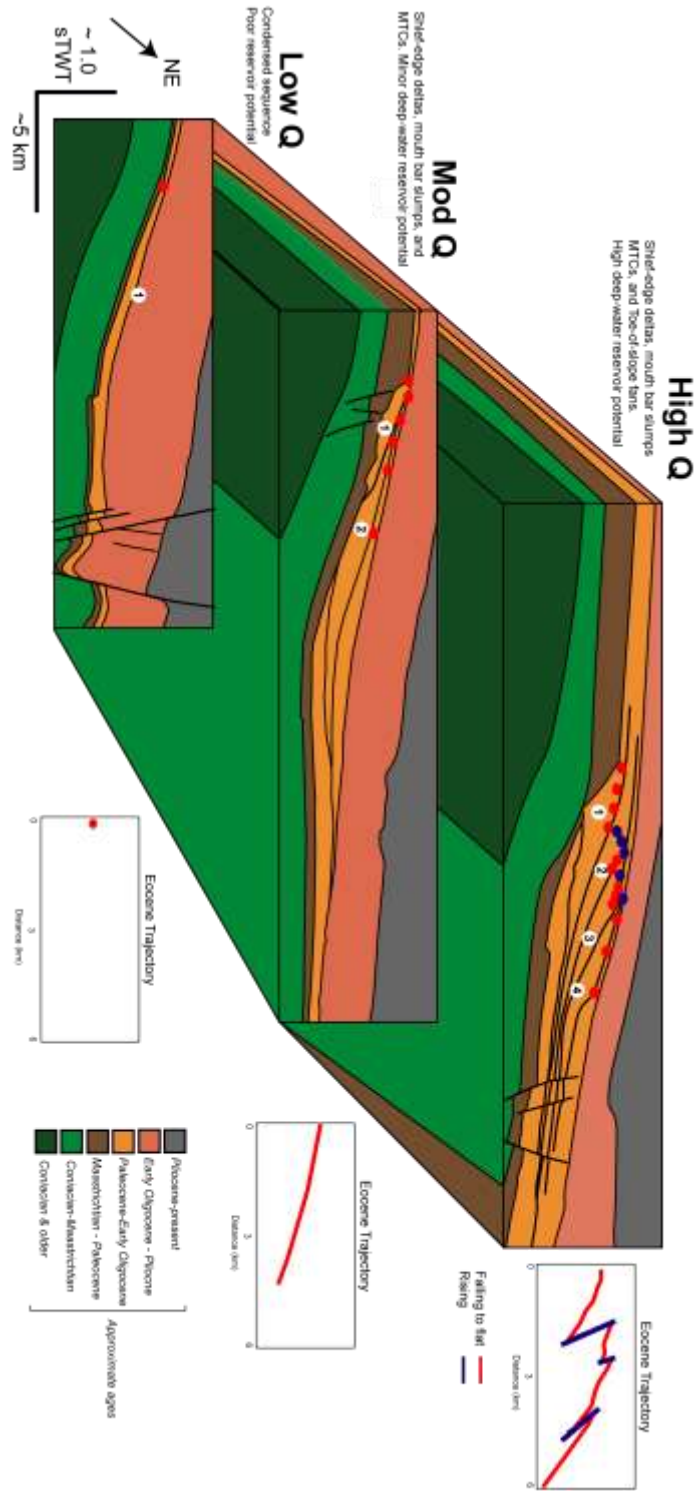


Figure 14: Synthesis of observations from high to moderate to low Q . Note significant differences in clinoform trajectory signature and related deep-water deposits along the shelf-edge.

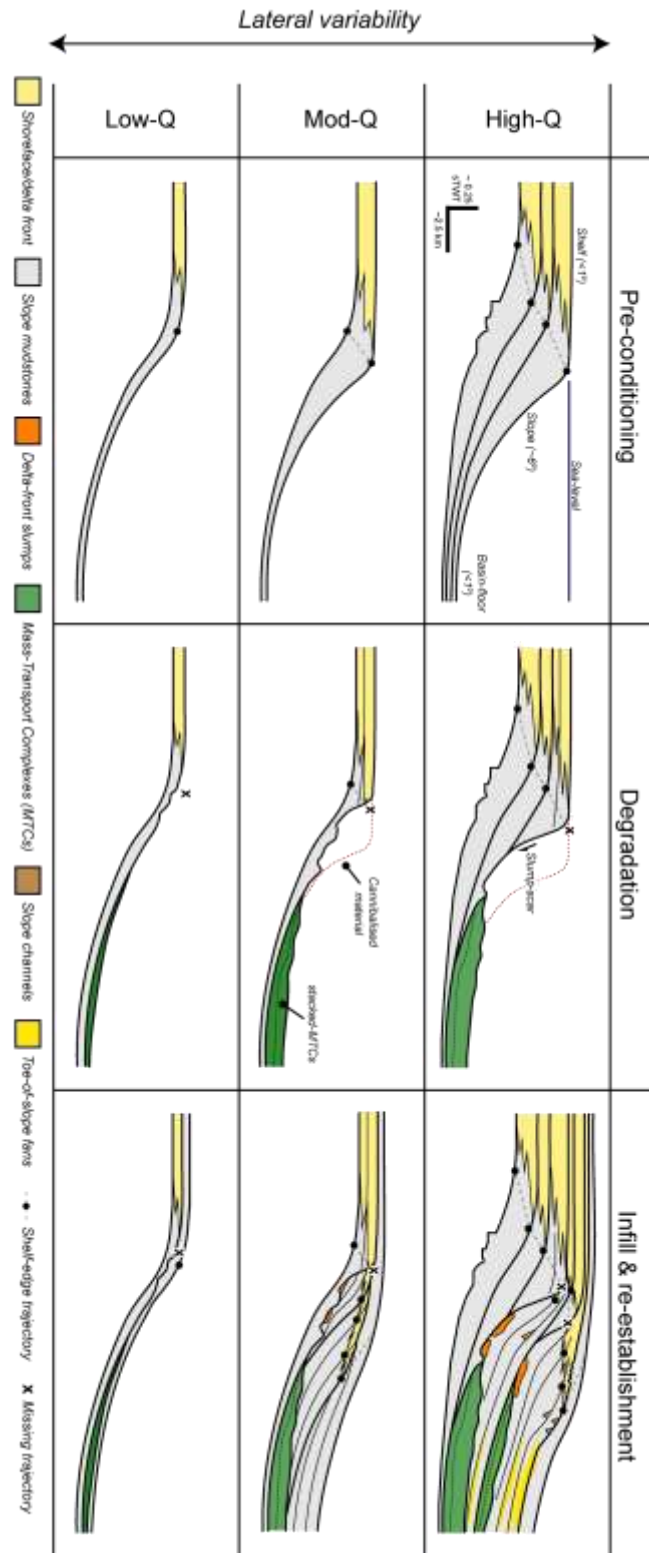


Figure 15: Conceptual model of along-strike variability and potential facies architectures to expect from high to moderate to low Q shelf-edge settings.

Table 1: Summary table of observed seismic facies and interpretations











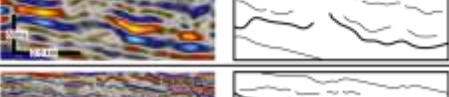

Seismic Facies	Description	Geometry	Location (Fig.2 Index)	Example	Interpretation
SF1	Sub-parallel, low-moderate amplitude, variable frequency and high continuity	Wedge W= >35km T= ~250ms L= >85km	Study wide Topset		Shelf
SF2	Low amplitude, low frequency and moderate continuity	Linear-Irregular W= 2-6.5km T= SR-100ms L= 14km	Northern Area Topset		Incised Valley Fill
SF3	High amplitude, variable frequency, low continuity	Sinuus W= SR-1.35km T= SR-50ms L= 10km	Northern Area Topset		Distributary Channels
SF4	High-low amplitude, moderate frequency, high continuity	Thin linear-sets W= 0.1-1km T= 20ms L= 28km	Northern & Central Area Topset		Beach Ridges/ Strandplain
SF5	High-low amplitude, moderate frequency, high continuity	Wide linear-sets W= 8km T= 75ms L= 28km	Northern & Central Area Topset		Foreshore/ Upper Shoreface
SF6	Low amplitude, low frequency, moderate continuity	Parallel-oblique clinoforms W= 7.8km T= SR-350ms L= 7.8km	Northern & Central Area Topset		Mid-Shelf Deltas
SF7	Low amplitude, high-moderate frequency, low-moderate continuity	Oblique sigmoidal to sigmoidal clinoforms W= up to 5km T= 75-150ms L=<0.15->1.5km	Northern & Central Area Foreset		Proto-Shelf -Edge Deltas
SF8	High-low amplitude, high-moderate frequency, high-moderate continuity	Oblique sigmoidal to sigmoidal clinoforms W= up to 20km T= 200-500ms L= 6-10km	Study wide Foreset		Shelf-Edge Deltas
SF9	High amplitude, high-moderate frequency, high-low continuity	Slope parallel elongate W= 75-200m T= 25-50ms L= 0.18-1.65km	Northern & Central Area Foreset		Slumps
SF10	High-low amplitude, moderate-low frequency, very low internal continuity, high bounding surfaces	Mounded W= up to 21km T= 75-600ms L= >27km	Study wide Bottomset		Mass-Transport Complex (MTC)
SF11	High amplitude, moderate-low frequency, moderate-low continuity	Sinuus W= SR-2km T=SR-40ms L=>10km	Northern Area Bottomset		Slope Channels
SF12	High amplitude, moderate-low frequency, high-moderate continuity	Strike-elongate lobate W= up to 3.5km T= SR-65ms L= 8km	Northern Area Bottomset		Toe-of-slope Fans

Table 2: Morphometric parameters observed in the Paleocene-Eocene seismic facies outlined in Table 1, VR = vertical resolution.

Facies	Morphometric Parameters				Examples
	Width (km)	Length (km)	Thickness (ms TWT)	Approx. thickness (m) assuming vel = 2750 ms ⁻¹	
SF1 (Shelf)	80+	35+	85-290	115-400	Fig. 4, 6, 9
SF2 (Incised Valley Fill)	2.00-6.5	14	VR-100	VR-140	Fig. 7
SF3 (Fluvial Channels)	0.05-1.35	11	VR-30	VR-40	Fig. 7
SF4 (Single Beach Ridges/Strandplain)	0.1-1.0	28+	20	28	Fig. 7, 8
SF5 (Foreshore/Upper Shoreface)	4-10	28+	40-75	55-105	Fig. 6
SF6 (Mid-Shelf Deltas)	7.8	4.25	175-350	240-480	Fig. 4, 5, 6
SF7 (Proto-Shelf-Edge Deltas)	5	2.75	75-150	105-205	Fig. 9
SF8 (Shelf-Edge Deltas)	20		200-500	275-685	Fig. 4, 9, 12
SF9 (Slumps)	0.18-1.65	0.075-0.2	25-50	35-70	Fig. 9, 10
SF10 (MTCs)	20	12+	75-275	105-375	Fig. 9, 10
SF11 (Slope Channels)	0.05-0.2	6+	VR-50	VR-70	Fig. 9, 11
SF12 (Toe-of-slope Fans)	3.5	6.75	VR-60	VR-83	Fig. 9, 11